PHILOSOPHICAL TRANSACTIONS OF THE ROYAL SOCIETY A MATHEMATICAL, PHYSICAL & ENGINEERING SCIENCES

A New Finite-Difference Solution-Adaptive Method

D. F. Hawken, J. S. Hansen and J. J. Gottlieb

Phil. Trans. R. Soc. Lond. A 1992 **341**, 373-410
doi: 10.1098/rsta.1992.0109

A new finite-difference solution-adaptive method

By D. F. Hawken†, J. S. Hansen and J. J. Gottlieb

Institute for Aerospace Studies, University of Toronto, Toronto, Ontario, Canada M3H 5T6

Contents

A new moving finite difference (MFD) method has been developed for solving hyperbolic partial differential equations and is compared with the moving finite element (MFD) method of K. Miller and R. N. Miller. These methods involve the adaptive movement of nodes so as to reduce the number of nodes needed to solve a problem; they are applicable to the solution of non-stationary flow problems that contain moving regions of rapid change in the flow variables, surrounded by regions

† Permanent address: High Speed Aerodynamics Laboratory, Uplands (U66), Institute for Aerospace Research, National Research Council, Montreal Road, Ottawa, Ontario, Canada K1A 0R6.

Phil. Trans. R. Soc. Lond. A (1992) **341**, 373–410
Printed in Great Britain

of relatively smooth variation. Both methods solve simultaneously for the flow variables and the node locations at each time-step, and they move the nodes so as to minimize an 'error' measure that contains a function of the time derivatives of the solution. This error measure is manipulated to obtain a matrix equation for node velocities. Both methods make use of penalty functions to prevent node crossing. The penalty functions result in extra terms in the matrix equation that promote node repulsion by becoming large when node separation becomes small. Extensive work applying the MFE and MFD methods to one-dimensional gasdynamic problems has been conducted to evaluate their performance. The test problems include Burgers' equation, ideal viscid planar flow within a shock-tube, propagation of shock and rarefaction waves through area changes in ducts, and viscous transition through a contact surface and a shock.

1. Introduction

Two of the most widely used methods of discretizing partial differential equations (PDEs) are finite elements and finite differences. Finite-element and finite-difference methods that use uniformly spaced nodes often waste computational effort, because to obtain acceptable truncation errors in regions of large solution variation much smaller node separations than are necessary in regions of negligible solution variation must be used. In the case of flows containing moving shocks, contact surfaces and slip streams, only a very small portion of the domain requires small node separations; thus significant economies can be obtained by moving the nodes so that they remain concentrated about areas of large solution variation.

To resolve a viscous shock transition properly the node separation in the vicinity must be several times smaller than the shock thickness. The shock thickness is related to the value of the coefficients of the second-order spatial-derivative (or diffusion) terms in the PDEs, often being of the same order of magnitude as these coefficients when the PDEs are written in normalized form. Hence, as the coefficients of the second-order terms are reduced, the shock thickness is reduced also. Non-zero coefficients are required to prevent infinitely steep, and thus aphysical, shock fronts and allow a non-zero node separation within a properly modelled shock. For commonly modelled physical scales and gas viscosities, physically accurate coefficients are usually extremely small and are in practice replaced by larger coefficients to allow larger node separations to be used. The use of adaptive methods allows much smaller node separations, and hence much smaller (more physically realistic) coefficients and much thinner shocks, than can in general be accommodated by non-adaptive methods. The ability to use smaller coefficients in the second-order terms also results in a more realistic growth of the thickness of contact surfaces with time. It should be noted that much larger time-steps are possible when the nodes move with a shock wave than can be obtained with a fixed non-uniform grid; time derivatives evaluated in the moving frame tend to be constant or zero.

Reviews of the field of adaptive solution are given by Hawken (1990), Hawken *et al.* (1991), Thompson *et al.* (1982, 1985), Thompson (1984, 1985), Turkel (1983), Anderson (1983) and Eiseman (1987). As pointed out by Thompson (1984), an adaptive-node method must have several ingredients:

(*a*) an orderly method of numbering (or mapping) nodes distributed over the physical region of interest;

PHILOSOPHICAL TRANSACTIONS OF THE ROYAL SOCIETY A MATHEMATICAL, PHYSICAL & ENGINEERING SCIENCES

(*b*) a means of 'communicating' between nodes so that the distribution of nodes remains fairly regular as they are shifted;

(*c*) a means of representing the continuous solutions discretely and a means of evaluating the discrete values with sufficient accuracy;

(*d*) a measure of the error in the discrete values that bears some relation to the truncation error;

(*e*) a means of redistributing the nodes as indicated by the measure, so as to reduce solution error.

On a one-dimensional domain, a second-order, multi-component PDE may be written in the form

$$\left.\frac{\partial \boldsymbol{A}}{\partial t}\right|_X = \boldsymbol{F}\left[X, t, \boldsymbol{A}, \frac{\partial \boldsymbol{A}}{\partial X}, \frac{\partial^2 \boldsymbol{A}}{\partial X^2}\right], \tag{1}$$

where $\boldsymbol{A} = \boldsymbol{A}[X,t] = [A_1, A_2 \ldots A_K]$ is the K component solution, X is the spatial coordinate, t is the time coordinate, $\boldsymbol{F} = [F_1, F_2 \ldots F_k]$ is a K-component function containing spatial derivatives of second or lower order. The components of the solution should be normalized to avoid the numerical difficulties that may arise if two components differ by several orders of magnitude.

The physical domain is unevenly divided into N intervals by nodes labelled 0 to N. The amplitude of each component at node i is denoted by A_m^i and the position of each node by X^i. The two adaptive methods that are compared in this paper both minimize an error measure to obtain a value for the velocity of each node.

The nodes are redistributed to minimize or reduce the average (in some sense) value of the measure. In the type of problems that are solved herein, it is essential to compute the values of the gasdynamical variables and the node velocities simultaneously to achieve acceptable solution accuracy and time-step size.

2. The moving finite element method

Miller & Miller (1981) and Miller (1981) devised a finite-element-based solution-adaptive technique, which they call the moving finite element (MFE) method. The method has been further developed by Djomehri & Miller (1981), Gelinas *et al.* (1981, 1982*a*, *b*), Gelinas & Doss (1981, 1982, 1983), Djomehri (1983), and Miller (1983, 1986). In this method the error measure may be interpreted as being the square of the residual of the PDE written in finite-element form. Ordinary differential equations (ODEs) for the nodal value of the physical variable and the nodal coordinate are obtained by minimizing the integral of error measure over the spatial domain. A version of the MFE method was coded as part of the process which led to the development of the finite-difference solution-adaptive method introduced in this paper. A brief description of the MFE method follows.

Piecewise linear approximation functions for each component are defined by

$$A_m^h[X,t] = \sum_{i=0}^{N} A_m^i \alpha^i, \tag{2}$$

where α^i is a linear 'Hat' basis function defined by

$$\alpha^i[X] = \begin{cases} 0 & \text{if} \quad X < X^{i-1}, \\ (X - X^{i-1})/\Delta X^i & \text{if} \quad X^{i-1} \leqslant X < X^i, \\ (X^{i+1} - X)/\Delta X^{i+1} & \text{if} \quad X^i \leqslant X < X^{i+1}, \\ 0 & \text{if} \quad X^{i+1} \leqslant X, \end{cases} \tag{3}$$

PHILOSOPHICAL TRANSACTIONS OF THE ROYAL SOCIETY A MATHEMATICAL, PHYSICAL & ENGINEERING SCIENCES

where $\Delta X^i = X^i - X^{i-1}$. This is the simplest possible basis function and simplifies subsequent algebra. As a consequence of the choice of basis function α^i, it can be shown that the time derivative of A^h_m at a fixed spatial coordinate is given by

$$\left.\frac{\partial A^h_m}{\partial t}\right|_X = \sum_{i=0}^{N} \dot{A}^i_m \alpha^i + \sum_{i=0}^{N} \dot{X}^i \beta^i_m, \tag{4}$$

where $\dot{A}^i_m$ and $\dot{X}^i$ are the time derivative of component m of the solution at fixed node-number i and the time derivative of the position (velocity) of node i, respectively, and where β^i_m is a basis function for component m and is defined by

$$\beta^i_m[X] = \begin{cases} 0 & \text{if} \quad X < X^{i-1}, \\ -M^i_m \alpha^i & \text{if} \quad X^{i-1} \leqslant X < X^i, \\ -M^{i+1}_m \alpha^i & \text{if} \quad X^i \leqslant X < X^{i+1}, \\ 0 & \text{if} \quad X^{i+1} \leqslant X. \end{cases} \tag{5}$$

In the above,

$$M^i_m = \frac{\Delta A^i_m}{\Delta X^i} = \frac{A^i_m - A^{i-1}_m}{X^i - X^{i-1}} \tag{6}$$

is the slope of component m between nodes i and $i-1$. Note that β^i_m is a discontinuous function of X since M^i_m is discontinuous.

Values for the time derivatives at fixed node number are obtained by minimizing the integral, over the spatial domain, of an estimate of the discretization error. The integral of the sum of the weighted squares of the residuals of the differential equations,

$$I = \int_{X^0}^{X^N} \sum_{m=1}^{K} \omega_m \left[\left.\frac{\partial A^h_m}{\partial t}\right|_X - F_m \right]^2 \mathrm{d}X \tag{7}$$

is minimized, by requiring that for all components k at each node j

$$\partial I / \partial \dot{X}^j = \partial I / \partial \dot{A}^j_k = 0. \tag{8}$$

This minimization yields equations which may be rewritten in matrix form and solved as discussed in §4. The weighting constants ω_m are scalar factors usually of order unity. The nodes move so that the residual with the largest value of ω_m will tend to have the smallest magnitude. Note that integrals containing complex forms of F_m will be difficult to code and expensive to evaluate. Details of these difficulties are discussed by Hawken (1990).

3. The moving finite difference method

The moving finite difference (MFD) method began as an attempt to capture some of the computational advantages of the MFE method while avoiding the expense associated with the computation of integrals of more complex partial differential equation terms. In particular, any term that requires numerical integration in the MFE formulation will slow the code down considerably. A second, unforeseen advantage of the MFD method is the larger time-steps obtained for a given problem as compared to those obtained by the MFE method.

It is convenient to transform to a numerical coordinate system (ξ, t) that moves with the nodes and in which the nodes are equidistributed such that $\xi^i = i$. An extra

factor proportional to the node velocity will appear in the transformed PDEs. One may approximate the PDEs by applying spatial central differences at each node in order to obtain ordinary differential equations (ODEs) in time for the solution amplitudes at the nodes. These ODEs may be written as

$$\dot{A}^i_m - \dot{X}^i \frac{\delta A^i_m}{\delta X^i} = f^i_m, \tag{9}$$

where $\delta X^i = X^{i+1} - X^{i-1}$, $\delta A^i_m = A^{i+1}_m - A^{i-1}_m$, and f^i_m is the central difference approximation to F_m at node i.

A value for the velocity of each node must be supplied. In the case of the MFE method, there is a natural minimization based on the sum of the squares of the discretized PDEs. There is no such obvious strategy for an adaptive finite difference method. It is merely desirable that nodes be concentrated in regions of large variation of the solution.

Most adaptive finite-difference methods attempt to minimize an 'error' measure that contains a function, usually *ad hoc*, of the first or second derivatives of the solution. The error-measures have included the absolute value, square, or positive even power of the estimated truncation error of $\boldsymbol{A}$ or of the node-to-node change in $\boldsymbol{A}$ or of a function of the slope or second derivative of $\boldsymbol{A}$ in the spatial coordinate system. Such error measures do not contain time derivatives and thus do not directly result in equations for the node velocities.

One can devise special manipulations to obtain expressions for node velocities using the above error measures but it is preferable to start with measures that already contain time derivatives. A correctly designed error measure that contains time derivatives will indirectly monitor the variation of the right-hand side of equation (9) and adjust node spacing so that the finite differences contained therein will be accurate. The development of a minor variation in the solution may be the result of a major variation in the time derivative of the solution. A measure that includes monitoring of variation of the time derivative should thus be more sensitive to 'error' than one that only monitors variation of the solution. Attempts to use an error measure that does not contain time derivatives as a basis for computing node velocities have resulted in very nonlinear or complex algorithms (see, for instance, Hindman & Spencer 1983; Rai & Anderson, 1980, 1982).

(*a*) *Use of an error measure based on time derivatives of the solution*

In developing the MFD method the aim was to retain a number of MFE advantages in addition to the use of time derivatives in the error measure. The MFE method uses a block tridiagonal matrix equation that allows the motion of a node to be influenced by the motions of all the other nodes. The relatively small band width of the matrix results in economical assembly and solution of the matrix equations. Certain matrix coefficients include factors of slope so that the influence on the velocity of a given node by the velocities of other nodes is reduced in regions of small slope; the motions of nodes resolving one feature of the flow (shock, contact surface, rarefaction wave) are relatively uninfluenced by the motion of the nodes resolving some other flow feature separated by a region of relatively small spatial variation of the solution. The MFE formulation allows moving shock solutions where nodes with constant amplitude move with constant velocities in the interior of the domain but are able to react to the proximity of a solid boundary where amplitude at a given node must change

rapidly to follow the reflection of a shock. It is desirable that the MFD procedure should involve some sort of variational or minimization principle similar to that used in the MFE method but avoid the use of integration.

After a great deal of numerical experimentation the following error measure was initially developed:

$$I^i = \sum_{m=1}^{K} \omega_m[-\dot{A}_m^{i+1} + 2\dot{A}_m^i - \dot{A}_m^{i-1}]^2 + \omega_{K+1}[-\dot{X}^{i+1} + 2\dot{X}^i - \dot{X}^{i-1}]^2 \sum_{m=1}^{K} \omega_m \left[\frac{\delta A_m^i}{\delta X^i}\right]^2. \quad (10)$$

The first sum contains a measure of the node-to-node variation of the time derivative of node amplitudes; the solution component with the largest value of ω_m will tend to have the smallest node-to-node variation of time derivative. As in the MFE method, the values of ω_m are of the order of unity and their exact values are not critical. If ω_{K+1} is non-zero, the second sum will result in a small node-to-node change in node velocity wherever some component of the solution has a large slope.

To obtain values for the node velocities, I^i is minimized with respect to the node velocity. For the purpose of minimization, I^i is considered to be a function of the node velocity only, and hence the time derivatives of the node amplitudes are expanded as functions of the node velocity using (9). The equation for node velocity is obtained by requiring that

$$\mathrm{d}I^i/\mathrm{d}\dot{X}^i = 0. \quad (11)$$

The resulting equation for the velocity of node i is

$$\sum_{m=1}^{K} \omega_m[-\dot{A}_m^{i+1} + 2\dot{A}_m^i - \dot{A}_m^{i-1}]\frac{\delta A_m^i}{\delta X^i} + \omega_{K+1}[-\dot{X}^{i+1} + 2\dot{X}^i - \dot{X}^{i-1}] \sum_{m=1}^{K} \omega_m \left[\frac{\delta A_m^i}{\delta X^i}\right]^2 = f_{K+1}^i, \quad (12)$$

with $f_{K+1}^i = 0$. (f_{K+1}^i will be given non-zero values in developments to be described below.)

The constant ω_{K+1} can be set to zero with good results for many problems; the measure I^i then simply monitors the node-to-node variation of the time-derivative of node amplitude. In this case I^i can be zero in spite of a very large node-to-node variation of the time derivative of the solution at fixed X; consider nodes moving across a domain in step with a shock wave of constant amplitude. To obtain a measure that is more sensitive to the node-to-node variation of the solution one might use the sum of the squares of the node-to-node variation of the left-hand sides of the ODEs for each component given by (9). Unfortunately, the equation for node velocity that results from minimizing this measure is simply a linear combination of the left-hand sides of the original ODEs. The equation is very similar to (12) with ω_{K+1} set to -1 (the coefficients are identical wherever the solution has the same slope at three adjacent nodes). A compromise value of $\omega_{K+1} = -\frac{1}{2}$ gives an equation for node velocity that has some sensitivity to the variation of the time derivative of at fixed X but is still linearly independent of the right-hand side of (9). Other reasons why it is sometimes appropriate to set ω_{K+1} to $-\frac{1}{2}$ are given by Hawken (1990).

4. Matrix equations

Equation (12) for all i, in combination with equation (9) for all i and m (or the MFE equations generated by the minimization of the residual in (7)), comprise a system

of $(K+1)\times(N+1)$ equations. It is convenient at this point for purposes of clarity of illustration to specialize to a system of three PDEs ($K=3$); most of the gasdynamical problems whose solutions are illustrated herein were solved in terms of three principle variables (gas velocity, density, and temperature). If one defines two column-vectors of dimension $(3+1)\times(N+1)$,

$$\dot{\boldsymbol{U}} = [\dot{A}_1^0, \dot{A}_2^0, \dot{A}_3^0, \dot{X}^0, \ldots, \dot{A}_1^N, \dot{A}_2^N, \dot{A}_3^N, \dot{X}^N]^{\mathrm{T}}$$

as the vector of time derivatives of the unknowns at each time-step, and

$$\boldsymbol{E} = [f_1^0, f_2^0, f_3^0, f_4^0, \ldots, f_1^N, f_2^N, f_3^N, f_4^N]^{\mathrm{T}}$$

as the vector of right-hand sides (T is the transpose operator), then (9) and (12) can be put in the form

$$[D]\,\dot{\boldsymbol{U}} = \boldsymbol{E}, \tag{13}$$

where

$$[D] = \begin{bmatrix} [C] & [R^0] & & & & & \\ [L^1] & [C^1] & [R^1] & & & \mathbf{0} & \\ & [L^2] & [C^2] & [R^2] & & & \\ & & \ddots & \ddots & \ddots & & \\ & & & [L^i] & [C^i] & [R^i] & \\ & \mathbf{0} & & & \ddots & \ddots & \ddots \\ & & & & & [L^N] & [C^N] \end{bmatrix}$$

is a block tridiagonal matrix. The left, central and right submatrices are square matrices of dimension $(K+1)\times(K+1)$.

In the case of the MFE method, the submatrices for $K=3$ are given by

$$[L^i]_{\mathrm{MFE}} = \begin{bmatrix} \frac{1}{6}\Delta X^i & 0 & 0 & -\frac{1}{6}\Delta A_1^i \\ 0 & \frac{1}{6}\Delta X^i & 0 & -\frac{1}{6}\Delta A_2^i \\ 0 & 0 & \frac{1}{6}\Delta X^i & -\frac{1}{6}\Delta A_3^i \\ -\frac{1}{6}\omega_1\,\Delta A_1^i & -\frac{1}{6}\omega_2\,\Delta A_2^i & -\frac{1}{6}\omega_3\,\Delta A_3^i & \sum_{m=1}^{3}\frac{1}{6}\omega_m M_m^i\,\Delta A_m^i \end{bmatrix},$$

$[R^i]_{\mathrm{MFE}} = [L^{i+1}]_{\mathrm{MFE}}$, and $[C^i]_{\mathrm{MFE}} = 2[L^i]_{\mathrm{MFE}} + 2[R^i]_{\mathrm{MFE}}$. The components of $\boldsymbol{E}$ are computed using

$$f_m^i = \int_{X^0}^{X^N} \alpha^i F_m^i \,\mathrm{d}X \tag{14}$$

and

$$f_{K+1}^i = \sum_{m=1}^{K} \omega_m \int_{X^0}^{X^N} \beta_m^i F_m^i \,\mathrm{d}X. \tag{15}$$

Evaluations of these integrals are discussed in Hawken (1990), Miller (1981), Gelinas *et al.* (1981) and Djomehri (1983).

In the case of the MFD method, the submatrices for $K = 3$ are given by

$$[C^i]_{\mathrm{MFD}} = \begin{bmatrix} 1 & 0 & 0 & -\dfrac{\delta A_1^i}{\delta X^i} \\ 0 & 1 & 0 & -\dfrac{\delta A_2^i}{\delta X^i} \\ 0 & 0 & 1 & -\dfrac{\delta A_3^i}{\delta X^i} \\ 2\omega_1 \dfrac{\delta A_1^i}{\delta X^i} & 2\omega_2 \dfrac{\delta A_2^i}{\delta X^i} & 2\omega_3 \dfrac{\delta A_3^i}{\delta X^i} & 2\omega_4 \sum\limits_{m=1}^{3} \omega_m \left[\dfrac{\delta A_m^i}{\delta X^i}\right]^2 \end{bmatrix},$$

$$[L^i]_{\mathrm{MFD}} = \begin{bmatrix} 0 & 0 & 0 & 0 \\ 0 & 0 & 0 & 0 \\ 0 & 0 & 0 & 0 \\ -\omega_1 \dfrac{\delta A_1^i}{\delta X^i} & -\omega_2 \dfrac{\delta A_2^i}{\delta X^i} & -\omega_3 \dfrac{\delta A_3^i}{\delta X^i} & -\omega_4 \sum\limits_{m=1}^{3} \omega_m \left[\dfrac{\delta A_m^i}{\delta X^i}\right]^2 \end{bmatrix},$$

and $[R^i]_{\mathrm{MFD}} = [L^i]_{\mathrm{MFD}}$.

The matrix $[D]$ for the MFD method has certain similarities to that of the MFE method. The coefficients of $[D]$ for a given node are only influenced by the values of the solution and node coordinate at the given and adjacent nodes, which greatly simplifies the computation of jacobian matrices for both methods. The matrix coefficients of the MFD method are similar in form to those of the MFE method, except for an additional factor of node separation in the denominator. In both methods, the coefficients of the node velocities have an extra factor of slope as compared with the coefficients of the time derivatives of the amplitudes.

Since node separation may become very small, the matrix equation may become stiff (in particular when waves interact with stationary structures) and require the use of a stiff ODE solver. It is most efficient to use an implicit method that requires the periodic computation of the jacobian (or matrix of derivatives with respect to the components of $\boldsymbol{U}$) of $\boldsymbol{E} - \dot{\boldsymbol{U}}[D]$. Equation (13) is solved using an adaptation of the implicit multistep backward-difference predictor-corrector algorithm, EPISODE. Various versions of EPISODE, which is descended from the method of Gear (1971), are described in Byrne (1979), Hindmarsh (1979) and Byrne & Hindmarsh (1975). The solution at a time-level, predicted using interpolation of the solution from previous time-levels, is corrected using a matrix equation that incorporates the jacobian. Following the strategy of Miller (1981) and Gelinas *et al.* (1981), the EPISODE algorithm was modified so that in addition to the usual tolerance on the size of the correction to the solution (including the spatial coordinate) at each node, a less stringent tolerance is specified on the size of the correction to the value of node separation (set equal to ten times the former tolerance).

Direct solution of (13) is required at the initialization of time iterations and as one of the steps in the (relatively infrequent) computation the jacobian. For the MFD method in those instances, it is convenient to use (9) to eliminate the time derivatives of the node amplitudes from (12). Then one needs simply to solve a tridiagonal system of equations for the node velocities and use (9) again to obtain the resultant time derivatives of the node amplitudes. Since $[D]$ is not so sparse in the MFE method, it is necessary to manipulate the full block tridiagonal matrix.

It is necessary to specify boundary conditions to compute the solution at node 0. (The boundary at node N is treated in a similar manner.) The $(K+1)$st row of (13) is always replaced by

$$\dot{X}^0 = 0$$

at a boundary since the spatial coordinate of a boundary node is fixed. If A_m^0 is specified at a boundary, then the mth row ($m \leqslant K$) of (13) is replaced by

$$\dot{A}_m^0 = \text{corresponding value of time derivative.}$$

If A_m is not specified at the boundary, it is assumed that the slope of A_m is zero at the boundary; the mth row of (13) is approximated by assuming symmetry about the boundary for all components of $\boldsymbol{A}$ that have zero slope and antisymmetry about the boundary for all components of $\boldsymbol{A}$ that have specified values at the boundary.

5. The Ω terms for the MFD method

(*a*) *Failure of MFE method and simple MFD method on stationary problems*

The adaptive finite difference method that has been described up to this point has one failing. To distinguish it from later refinements, it will henceforth be called the simple MFD method.

The right-hand side of (12) is zero for the simple MFD method. Consider the special case where the right-hand side of (9) is zero for all components of $\boldsymbol{A}$ throughout the domain. In this case, the solution of the problem at any time is given by the initial values. All components of $\boldsymbol{E}$ in (13) are zero. A solution of the system of equations yields zero node velocities, even though there might be some benefit in moving the nodes so as to increase their concentration in regions where the solution has a larger error measure. The system of equations generated by the MFE method also yields zero node velocities when the right-hand sides of the PDEs are zero for all components of $\boldsymbol{A}$ throughout the domain.

In other words, the MFE and simple MFD methods assume that the initial conditions have a good node distribution and move the nodes thereafter to preserve this distribution in some sense. Extensive application of the MFE and simple MFD methods to a number of test PDEs has revealed that there is a strong tendency for the nodes to move along the solution characteristics. That is, the time derivatives of $\boldsymbol{A}$ at each node tend to be small relative to the node velocity in the interior of undisturbed moving shock and rarefaction waves. This tendency to follow characteristics is most easily understood in the case of the MFD method. Ignoring the effect of boundary conditions, examination of $[L^i]_{\text{MFD}}$, $[C^i]_{\text{MFD}}$, and $[R^i]_{\text{MFD}}$ should make it clear that if each node moves at the local characteristic velocity so that the components of the solution are constant at the node, the MFD matrix equation will be satisfied whenever the velocity of a node is the average of the node velocity at the two adjacent nodes (if ω_4 is zero the second condition is not required but is satisfied anyway to a fairly good approximation). There is no provision in the MFE or simple MFD methods to prevent nodes from drifting away from optimum positions or to attract them into more optimal positions. For instance, consider the problem of a rarefaction wave transmitted through an area reduction in a duct. If a recompression or stationary shock forms within the area change, the tendency of the nodes to follow the characteristics is so strong that few nodes remain within this stationary shock.

(b) Improvement of MFD method by use of solution-based error measure

In problems that contain stationary waves of constant profile, the problem described above can be alleviated by adding a measure containing a spatial variation of the solution to the measure containing a spatial variation of the time derivative given by (10). There should be a component of time derivative in this new measure so that the derivative with respect to node velocity will be non-zero and the functional form of the new measure should be similar to that of (10). One possibility is to replace the time derivatives in (10) by an average of the solution at the present and next time-steps.

The result of the replacement is

$$I^i_\Omega = \sum_{m=1}^{K} \omega_m[-\bar{A}^{i+1}_m + 2\bar{A}^i_m - \bar{A}^{i-1}_m]^2 + \omega_{K+1}[-\bar{X}^{i+1} + 2\bar{X}^i - \bar{X}^{i-1}]^2 \sum_{m=1}^{K} \omega_m \left[\frac{\delta A^i_m}{\delta X^i}\right]^2, \quad (16)$$

where

$$\bar{X}^i = X^i + \tfrac{1}{2}\Delta t \dot{X}^i \quad \text{and} \quad \bar{A}^i_m = A^i_m + \tfrac{1}{2}\Delta t \dot{A}^i_m \quad (17)$$

are approximations to the time averages, with Δt being the size of the time-step.

A linear combination of (16) and (10) produces an improved measure that contains a weighted influence from the spatial variation of the solution averages. Equation (16) is multiplied by $\Omega/\Delta t$, where Ω is the weighting constant, and the result is added to (10). The equation for node velocity is obtained by writing the composite measure as a function of node velocity only, using (9) and (17) and requiring that

$$\mathrm{d}(I^i + (\Omega/\Delta t) I^i_\Omega)/\mathrm{d}\dot{X}^i = 0. \quad (18)$$

The result divided by $[1 + \frac{1}{4}\Omega\,\Delta t]$ is identical to (12) except that f^i_{K+1} is no longer zero but is given by

$$f^i_{K+1} = \tfrac{1}{2}\bar{\Omega} \sum_{m=1}^{K} \omega_m[A^{i+1}_m - 2A^i_m + A^{i-1}_m] \frac{\delta A^i_m}{\delta X^i} + \tfrac{1}{2}\omega_4 \bar{\Omega}[X^{i+1} - 2X^i + X^{i-1}] \sum_{m=1}^{K} \omega_m \left[\frac{\delta A^i_m}{\delta X^i}\right]^2, \quad (19)$$

where $\bar{\Omega} = \Omega/[1 + \frac{1}{4}\Omega\,\Delta t]$. The above will be referred to as the 'Ω terms' hereafter.

For sufficiently small Ω and Δt, the Ω terms will have negligible dependence on the time-step size. The weighting constant Ω chosen should be small enough so that the influence of solution spatial variation will become important only if the time derivatives become quite small, as in a stationary wave of constant profile. Excessively large values of Ω will reduce the time-step size without improving solution quality.

6. Penalty-function terms and other MFE refinements

Penalty functions were introduced by Miller (1981) and Miller & Miller (1981), and further developed by Gelinas *et al.* (1981), Djomehri (1983) and Miller (1983), as a means of preventing nodes from crossing each other in regions of large solution variation, and also to prevent singularity of the matrices associated with the MFE method. (Examination of the MFE submatrices reveals that their rows are linearly dependent in regions of uniform slope, that is, regions where the slope is the same in adjacent elements.) These penalty functions have been adopted, in modified form, for use in the MFD method. In both the MFE and the MFD methods there is a tendency for the nodes to concentrate excessively in the interiors of shock waves since the nodes tend to follow the characteristics, which coalesce in a shock (and cross for

inviscid problems). Extra terms are inserted into the MFE and MFD equations used for calculating the node velocities (every $(K+1)$th row of (13)). These terms become dominant when the nodes are very close together and in addition prevent degeneracy of the system of equations in regions of zero slope (and, in case of the MFE method, in regions of uniform slope). The extra terms are the result of minimizing the following measure of relative node velocity and node position,

$$I_p = \sum_{j=1}^{N} [e^j[\dot{X}^j - \dot{X}^{j-1}] - s^j]^2, \tag{20}$$

by requiring that

$$\partial I_p / \partial \dot{X}^i = 0 \tag{21}$$

for all nodes i. In this measure, e^i and s^i are positive functions of ΔX^i and are defined in such a way that they become very large when ΔX^i is very small or approaches some specified minimum value. Under such conditions the change in node velocity from node to node will approach a value dictated by the ratio of s^i to e^i.

The result of the minimization,

$$-\dot{X}^{i-1}e^ie^i + \dot{X}^i[e^ie^i + e^{i+1}e^{i+1}] - \dot{X}^{i+1}e^{i+1}e^{i+1} = e^is^i - e^{i+1}s^{i+1}, \tag{22}$$

is added to the MFE and MFD equations for calculating the velocity of each node i.

Various types of penalty function have been used. Gradient weighted penalty functions, originally introduced by Gelinas & Doss (1981), have proven to be the most straightforward and convenient to use. The present formulation, where

$$e^ie^i = C_3\left[1 + C_G \sum_{m=1}^{K}\left[\frac{\Delta A^i_m}{\Delta X^i}\right]^2\right] \Big/ [\Delta X^i - C_0]^{C_5} \tag{23}$$

and

$$e^is^i = C_2/[\Delta X^i - C_0]^{C_4}, \tag{24}$$

and the methods of choosing initial trial values for the weights C_3, C_G, C_2 are based on the work of Djomehri (1983). The coefficients of node velocity in the equation for calculating the velocity of node i vary as $[\Delta A^i_m]^2/[\Delta X^i]$ for the MFE method and as $[\delta A^i_m]^2/[\delta X^i]^2$ for the MFD method. C_5 is set to 1 for the MFE method and to 2 for the MFD method to obtain matching variation of e^ie^i with node separation. C_0, the minimum node spacing, may be set to zero in most cases. C_3 is chosen to be 20 or 30 times larger than the square of the allowable spatial truncation error so that e^ie^i only becomes important if $[\Delta A^i_m]^2$ is relatively small. The gradient weighting in (23) causes e^ie^i to become very large within regions of large slope and thus prevents the rapid expulsion of nodes from the interiors of shocks that occurs in some cases; C_G has ranged from 10^{-2} to 10^{-3} when not set to zero.

It can be shown that second-order spatial derivatives (arising from diffusion processes) substituted into the integral of (15) result in terms of the form $[\Delta A^i_m/\Delta X^i]^2 - [\Delta A^{i+1}_m/\Delta X^{i+1}]^2$ in the MFE equation for calculating the velocity of node i. These terms tend to prevent node crossing and hence have an effect complementary to that of the e^is^i terms. For the MFE method, C_4 is set to 2 and C_2 is chosen to be 20 or 30 times smaller than the square of allowable spatial truncation error multiplied by the diffusion coefficient so diffusion terms will dominate $e^is^i - e^{i+1}s^{i+1}$ unless $[\Delta A^i_m]^2$ is very small for all components of the solution. The same form of the e^is^i terms has been retained for the MFD method but C_4 is increased to 3 to provide a better balance with the larger value of C_5.

The considerable numerical experimentation required to obtain optimum final values for the penalty-function weights represents the most difficult task in using the

MFE and MFD methods. Note that the penalty functions do not enhance adaptivity but are included to prevent singularity of the matrices, node crossing, and excessive entry of nodes into the interiors of shocks.

A number of ways, in addition to the use of penalty functions, of improving performance have been developed by the authors of the MFE method. Two of these methods, overemphasis of diffusion and horizontal emphasis, have been implemented in the code and are discussed below.

It is shown by Djomehri (1983) and Miller (1983) that if penalty functions are not used then all the nodes tend to move into the interior of a shock, causing insufficient resolution at the top and bottom of the shock. Only MFE terms resulting from second-order spatial derivatives in the PDEs tend to oppose this motion, but they are unable to push the nodes out of the shock because the diffusion coefficients are generally too small. Djomehri (1983) and Miller (1983) improved the beneficial effects of the diffusion terms by multiplying any second-order spatial derivative term included in the integrals in (15) by the scalar factor $1+D$, where D represents the 'amount' of overemphasis of diffusion. They show, using some model equations, that $1 > D \geqslant 0$ is a sufficient condition to obtain a monotone solution near a shock. The use of overemphasis of diffusion makes it easier to choose penalty-function coefficients that will prevent all the nodes from entering a shock without driving too many nodes out of the shock.

Djomehri (1983) has modified the MFE equations so that changes in X^i are more important than changes in the magnitude of $\boldsymbol{A}^i$ (terms horizontal and vertical movement, respectively, by Djomehri) in minimizing the integrals of the residuals. The MFE equations remain the same except that, in the bottom row of each MFE submatrix, the coefficients of the time derivatives of the components of $\boldsymbol{A}$ at each node are multiplied by a scalar horizontal emphasis parameter. A horizontal emphasis parameter value of one yields the original MFE method, while a value of zero causes the node velocities to be uninfluenced by the time derivatives of $\boldsymbol{A}$. The use of a horizontal emphasis parameter with a value less than unity reinforces the tendency of the MFE method to produce 'travelling wave' solutions in which the nodes travel with the wave with essentially no change in the value of $\boldsymbol{A}$ at each node. Any tendency of nodes at the front end of a shock to drift or creep back through the shock is reduced. As added benefits, the nearly constant time derivatives at each node result in much larger time-steps and the positive definiteness of $[D]$, and therefore the stability of the MFE equations is enhanced.

7. Alternative Ω terms derived from minimization of an error measure

It is possible to obtain an alternative to the Ω terms of (19) by using the calculus of variations. The following has been inspired by the work of Hindman & Spencer (1983).

The integral of an error measure

$$I = \int_{X^0}^{X^N} \left[\frac{\lambda}{\alpha} \left[\frac{\partial \xi}{\partial X} \right]^{\alpha} + \frac{W}{\beta} \left[\frac{\partial X}{\partial \xi} \right]^{\beta} \right] \mathrm{d}X \tag{25}$$

is to be minimized. W is a measure of solution variation and α, β, and λ are scalar constants. ξ is a computational coordinate chosen so that ξ^i is equal to i. The power α exceeds 1, whereas β exceeds 0. In the method of Hindman & Spencer, they were set to 2 and 1 respectively. The first term in the integrand promotes smoothness of

the transformation, whereas the second term promotes concentration of nodes in regions with a large value of W. In contrast with the method of Hindman & Spencer, where W was defined to be $[\partial A/\partial\xi]^2$ for a single component problem, here W, in its simplest form, will be $[\partial A/\partial X]^2$. The calculus of variations is applied to the integral to yield the Euler equation

$$\left[\frac{\partial}{\partial\xi}-\frac{\mathrm{d}}{\mathrm{d}X}\frac{\partial}{\partial[\partial\xi/\partial X]}\right]\left[\frac{\lambda}{\alpha}\left[\frac{\partial\xi}{\partial X}\right]^{\alpha}+\frac{W(X)}{\beta}\left[\frac{\partial X}{\partial\xi}\right]^{\beta}\right]. \tag{26}$$

The solution of the Euler equation,

$$\lambda\left[\frac{\partial X}{\partial\xi}\right]^{1-\alpha}-W\left[\frac{\partial X}{\partial\xi}\right]^{1+\beta}=\text{const.}, \tag{27}$$

is differentiated with respect to ξ and divided by $[\partial X/\partial\xi]^{\beta}$ to obtain

$$-[\alpha-1]\lambda\frac{\partial^2 X}{\partial\xi^2}\left[\frac{\partial X}{\partial\xi}\right]^{-\alpha-\beta}-[\beta+1]W\frac{\partial^2 X}{\partial\xi^2}+\frac{\partial W}{\partial\xi}\frac{\partial W}{\partial\xi}=0. \tag{28}$$

To reduce nonlinearity in subsequent equations, the equation above will not be rewritten in the 'forcing function' form of Hindman & Spencer. Instead, the equation is approximated at each node i by using central differences to obtain

$$-[\alpha-1]\lambda\frac{X^{i+1}-2X^i+X^{i-1}}{[\frac{1}{2}\delta X^i]^{\alpha+\beta}}-[\beta+1]\frac{W^{i+\frac{1}{2}}+W^{i-\frac{1}{2}}}{2}[X^{i+1}-2X^i+X^{i-1}]$$
$$-\frac{W^{i+\frac{1}{2}}-W^{i-\frac{1}{2}}}{1}\frac{X^{i+1}-X^{i-1}}{2}=0. \tag{29}$$

Here $W^{i+\frac{1}{2}}$ and $W^{i-\frac{1}{2}}$ are estimates of W in the middle of the interval to each side of node i and are defined by

$$W^{i+\frac{1}{2}}=\sum_{m=1}^{K}\omega_m\left[\frac{\Delta A_m^{i+1}}{\Delta X^{i+1}}\right]^2.$$

Note that nodes will tend to equidistribute in regions of uniform slope, thereby reducing spatial truncation error. The value of W at node i has been approximated as an average of $W^{i+\frac{1}{2}}$ and $W^{i-\frac{1}{2}}$, and the derivative of W with respect to ξ has been approximated by the difference divided by $\xi^{i+\frac{1}{2}}-\xi^{i-\frac{1}{2}}=1$.

Equation (29) can be rearranged to resemble the right-hand side of the MFD equation for node velocities including penalty terms and Ω terms. The term proportional to λ corresponds to an alternative form of $e^i s^i-e^{i+1}s^{i+1}$; the value of α may be chosen so that $\alpha+\beta$ is an integer. As detailed in Hawken (1990), two forms of this term gives rise to alternative penalty terms that are inferior in performance to the penalty terms described in §6. The rest of the terms in (29) may be rearranged to resemble the Ω terms of (19).

By rearranging (29), setting λ to zero, dividing by $\beta+2$, and introducing the weighting constant Ω', an alternative form of the Ω terms,

$$f_{K+1}^i=\tfrac{1}{2}\Omega'\Delta X^{i+1}\left[\sum_{m=1}^{3}\omega_m\left[\frac{\Delta A_m^{i+1}}{\Delta X^{i+1}}\right]^2+B\sum_{m=1}^{3}\omega_m\left[\frac{\Delta A_m^{i}}{\Delta X^{i}}\right]^2\right]$$
$$-\tfrac{1}{2}\Omega'\Delta X^i\left[B\sum_{m=1}^{3}\omega_m\left[\frac{\Delta A_m^{i+1}}{\Delta X^{i+1}}\right]^2+\sum_{m=1}^{3}\omega_m\left[\frac{\Delta A_m^{i}}{\Delta X^{i}}\right]^2\right], \tag{30}$$

is obtained, where $B = \beta/[\beta+2]$. Details of the derivation of, and justification for, (30) are provided in Hawken (1990).

Equation (29) may also be written in the form

$$\frac{\Delta X^{i+1}}{\Delta X^i} = \frac{\{[\alpha-1]\,L/[\frac{1}{2}\delta X^i]^{\alpha+\beta}\}+\frac{1}{2}BW^{i+\frac{1}{2}}+\frac{1}{2}W^{i-\frac{1}{2}}}{\{[\alpha-1]\,L/[\frac{1}{2}\delta X^i]^{\alpha+\beta}\}+\frac{1}{2}W^{i+\frac{1}{2}}+\frac{1}{2}BW^{i-\frac{1}{2}}}, \tag{31}$$

where $L = \lambda/[\beta+2]$. It is easily seen that, if (29) is satisfied, X^i lies between X^{i+1} and X^{i-1} for non-zero L. When L is zero, it is apparent that $\Delta X^{i+1}/\Delta X^i \sim B$ if $W^{i+\frac{1}{2}}$ is much larger than $W^{i-\frac{1}{2}}$ and that $\Delta X^i/\Delta X^{i+1} \sim B$ if $W^{i-\frac{1}{2}}$ is much larger than $W^{i+\frac{1}{2}}$. Therefore the value of β places a limit on the maximum ratio of node separation in regions of non-zero slope. Larger values of β will cause an increased averaging of the estimates of W and increase the order of spatial truncation error as the maximum ratio of node separation approaches one but will reduce the adaptivity of the nodes. If $1 > \beta > 0$, then a very large maximum node separation ratio may occur. The quantity B is called the 'maximum-ratio-of-node-separation parameter' in this paper.

Use of the Ω terms complicates selection of penalty-function weights. However, two rules have been found to be of use. If Ω' is of the order of unity, then the penalty-function coefficients should be close to those used for zero Ω', except that C_2 should be about 20% larger. For larger values of Ω', doubling Ω' requires an approximate doubling of C_2 and C_3, with C_2 increased about 20% more than C_3. One initially uses a value of zero for Ω'. Then, if necessary, the results of using progressively larger values of Ω' are compared to the best result with zero Ω'.

A similar rule has been discovered for variation of Reynolds number. If the Reynolds number based on the speed of sound is halved, then C_2 and C_3 should be approximately doubled, with C_2 increased about 20% more than C_3 to increase node spread.

The results of the MFD method given by (9) and (12) with non-zero Ω terms will be compared to the results of the MFE method in §§8–11. Specification of the value of B provides an influence on the variation of node spacing throughout the domain. An optimal value of B for the problems solved appears to be *ca.* $\frac{1}{4}$. Use of non-zero Ω' generally provides a higher-quality solution than use of non-zero $\bar{\Omega}$. The value that gives the best results for $\bar{\Omega}$ generally is close to the value that gives the best results for Ω' if $B \approx \frac{1}{4}$. Tolerances per time-step of 10^{-4} on X and each component of $\boldsymbol{A}$ and of 10^{-3} on the node separation were specified in all cases. All the calculations were performed on a Perkin Elmer 3250 minicomputer.

8. Burgers' equation test problem

This test problem is based on that of Miller (1981). It consists of the adaptive solution, on the domain 0–1, of Burgers' equation,

$$\frac{\partial U}{\partial t} = -U\frac{\partial U}{\partial X}+\frac{1}{2}\delta\frac{\partial^2 U}{\partial X^2}, \tag{32}$$

introduced by Burgers (1948). The initial values of U at each node are given by $U^i = \frac{1}{2}\sin(\pi X^i)+\sin(2\pi X^i)$. The Dirichlet condition, $U = 0$, is applied at $X = 0$ and $X = 1$ and $\frac{1}{2}\delta$ is set to 10^{-3}.

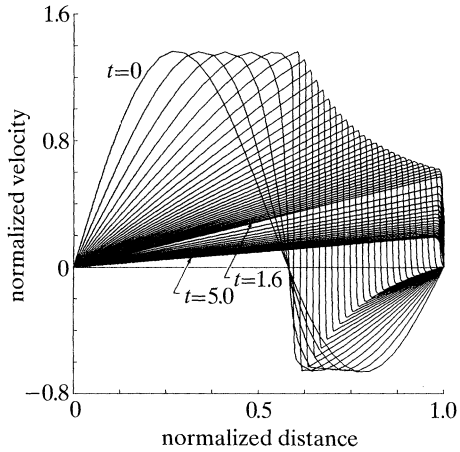

Figure 1. Profiles from the standard MFD solution of Burgers' equation from $t = 0$ to $t = 5$. $\Delta t = 0.05$ from $t = 0$ to $t = 1.6$ and $\Delta t = 0.2$ thereafter. Parameters: 31 nodes, $C_0 = 0$, $C_2 = 1.25 \times 10^{-10}$, $C_3 = 4.8 \times 10^{-8}$, $C_4 = 3$, $C_5 = 2$, $\Omega' = 1.5$, $B = 0.25$, $\omega_1 = 1$, $\omega_2 = -0.5$.

(*a*) *Results of* MFD *calculations*

The MFD method was applied to Burgers' equation using 31 nodes that were initially equidistributed. The solution weight ω_1 was set to one, and ω_2 was set to $-\frac{1}{2}$. Ω' and the maximum-ratio-of-node-separation parameter B were set to 1.5 and $\frac{1}{4}$ respectively. The penalty-function coefficients were $C_0 = 0$, $C_2 = 1.25 \times 10^{-10}$, $C_3 = 4.8 \times 10^{-8}$ and $C_G = 0$ with powers $C_4 = 3$ and $C_5 = 2$. The calculation described above will be referred to, in what follows, as the 'standard MFD calculation'.

The resultant profiles of U at various times from $t = 0$ to $t = 5$ are shown in figure 1. A wave sweeps to the right and steepens into a shock whose amplitude decays as it continues to sweep to the right. The shock eventually reaches the right-hand end of the domain and further decays *in situ*. The entire calculation took about two CPU minutes and required the computation of 46 jacobians and a total of 766 finite-difference evaluations of the right-hand side of (13). Since the calculation was implicit, the size of the time-step exceeded the linear CFL limit by factors as large as 853 as the shock decayed after reaching the end of the domain. The final value of Δt, at $t = 5$, was 0.32, and the fraction of the total integration-time span that used the first-, second-, third- and fourth-order EPISODE ODE-solution methods were about 0.8%, 18%, 77% and 5% respectively. The CPU time increases by a factor of at least 13 if functional iterations, which do not use a jacobian, are used. Figure 2*a*, *b* illustrates the node distribution at various times during the calculation. It can be seen that the nodes round out the corners as is desirable. Similar results occur if $\Omega = 1.5$ is used instead of Ω'. If the number of nodes is reduced to 21, unacceptable kinking occurs.

Increasing C_2 increases node separation, driving nodes out of the shock, but it does not increase node concentration at the corners; increasing C_3 reduces the node spread, allowing more nodes to enter the shock, without appreciably increasing the node concentration at the corners. Increasing C_2 and C_3 together increases the node-to-node change in U within the shock and may increase execution speed, but excessive values will cause oscillations at the corners as nodes are driven apart. Similar behaviour resulted for the test problems discussed in §§9–11.

If the standard MFD calculation is repeated with $\Omega' = 2$, too many nodes enter the

PHILOSOPHICAL TRANSACTIONS OF THE ROYAL SOCIETY A MATHEMATICAL, PHYSICAL & ENGINEERING SCIENCES

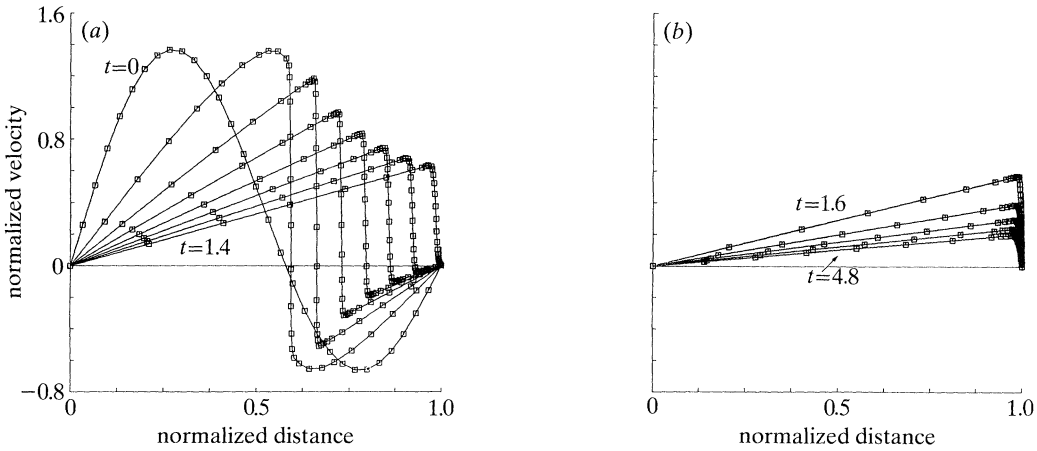

Figure 2. Typical node distributions corresponding to the profiles of figure 1 for (*a*) $t = 0$, 0.2, 0.4, 0.6, 0.8, 1.0, 1.2 and 1.4; and (*b*) $t = 1.6$, 2.4, 3.2, 4.0 and 4.8.

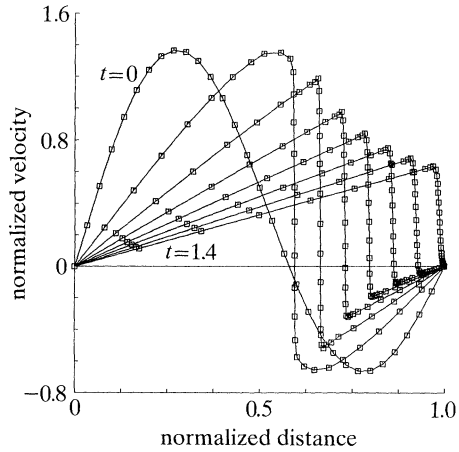

Figure 3. Node distributions at $t = 0$, 0.2, 0.4, 0.6, 0.8, 1.0, 1.2 and 1.4 if the standard MFD solution of Burgers' equation is repeated with ω_2 changed from -0.5 to 0 and if the resultant node distribution is improved by reducing Ω' from 1.5 to 1.

shock, leaving too few to round out the corners. If Ω' is set to $\frac{1}{2}$, the nodes do not enter quite so far into the shock and do not round out the corners as well as in the standard MFD calculation. Setting Ω' to zero results in severe kinking at the top of the shock.

If the standard MFD calculation is repeated with $\omega_2 = 0$, too many nodes enter the shock and concentration of nodes is greatly reduced at the top corner of the shock. Reducing Ω' to unity improves matters slightly but still leaves small kinks at the top and bottom of the shock due to the poor node concentration, as shown in figure 3. Adjustments of other parameters do not improve matters.

The standard MFD calculation was repeated with the advection term written in conservation law form:

$$\frac{\partial U}{\partial t} = -\frac{1}{2}\frac{\partial U^2}{\partial X} + \tfrac{1}{2}\delta\frac{\partial^2 U}{\partial X^2}. \tag{33}$$

The results are of similar quality but the shock decays more slowly and moves more quickly. The CPU time was about the same.

PHILOSOPHICAL TRANSACTIONS OF THE ROYAL SOCIETY A MATHEMATICAL, PHYSICAL & ENGINEERING SCIENCES

(*b*) *Results of* MFE *calculations*

The MFE method was applied to the Burgers' test problem with the same number of nodes. The solution weight was $\omega_1 = 1$. The penalty-function coefficients were $C_0 = 10^{-3}$, $C_2 = 2 \times 10^{-9}$, $C_3 = 8 \times 10^{-5}$, and $C_G = 0$ with powers $C_4 = 2$ and $C_5 = 1$. The calculation described above will be referred to, in what follows, as the 'standard MFE calculation'.

The resulting profiles agreed well with those of the MFD calculations and, as illustrated in figure 4, the typical node distributions were reasonably close to those obtained by the MFD method. The MFE CPU time was more than twice that of the MFD method and required the computation of 196 jacobians and a total of 2472 finite-element evaluations of the right-hand side of (13). The reason why the MFD calculation is not about four times faster than the MFE calculation, as would be implied by the ratio of jacobian evaluations or of right-hand side evaluations, is that the MFD code is experimental and contains many options that increase flexibility at the expense of execution efficiency. The speed advantage of the experimental MFD code becomes more pronounced as the number of nodes and number of PDEs are increased.

As the shock decayed after reaching the end of the domain, the size of the time-step exceeded the linear CFL limit by factors as large as 54; the larger Courant numbers obtained by the MFD method were the result of generally larger time-steps and smaller node separations. The final value of Δt, at $t = 5$, was 0.31, and the fractions of the total integration-time span that employed the first-, second-, third- and fourth-order EPISODE ODE-solution methods were about 0.08 %, 7 %, 66 % and 27 % respectively. If functional iterations are used, the MFE computation fails to reach $t = 0.25$, despite the use of 5000 evaluations of (13).

If the number of nodes is reduced to 21, the CPU time is reduced to about the same as that of the MFD solution, but not quite enough nodes are forced out of the shock to prevent kinking at the top and bottom of the shock. Increasing C_0 to 2×10^{-3} greatly improves the results. As shown by comparison of figures 4 and 5, there is no visible reduction in quality relative to a calculation using 31 nodes. The MFE method is much more tolerant of large changes in slope between elements than is the MFD method. As mentioned earlier, unacceptable kinking occurs near the top of the shock, if Burgers' equation is solved with 21 nodes using the MFD method.

The standard MFE calculation was repeated with the convective term written in conservation-law form. Unfortunately, the CPU time was much larger than for the nonconservation-law form. Although no evidence of instability was seen up to $t = 0.15$, the time-integration did not proceed to $t = 0.2$ despite the use of 5000 finite-element evaluations of the right-hand side of (13). A number of parameters were varied, but no improvement was obtained.

9. Shock-tube problem

A shock tube with closed ends containing air initially with a uniform temperature and zero velocity is illustrated in figure 6. At the start of the problem, the air in the driver section of the shock tube (to the left of a diaphragm) is at twice atmospheric pressure, whereas the air in the region to the right of the diaphragm is at atmospheric pressure. Upon removal of the diaphragm a rarefaction wave proceeds to the left and

Figure 4

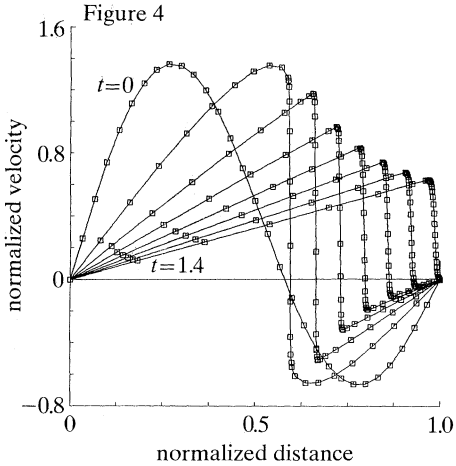

Figure 5

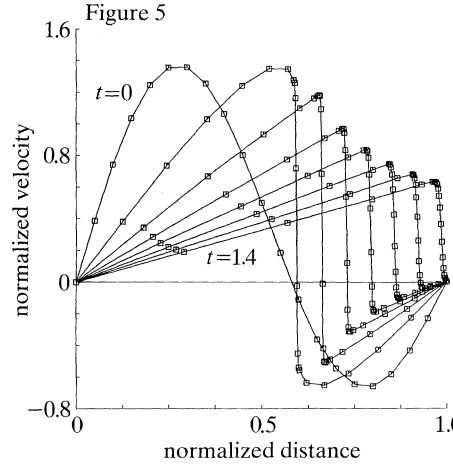

Figure 4. Node distributions from the standard MFE solution of Burgers' equation for $t = 0$, 0.2, 0.4, 0.6, 0.8, 1.0, 1.2 and 1.4. Parameters: 31 nodes, $C_0 = 1 \times 10^{-3}$, $C_2 = 2 \times 10^{-9}$, $C_3 = 8 \times 10^{-5}$, $C_4 = 2$, $C_5 = 1$, $\omega_1 = 1$.

Figure 5. Node distributions that occur for $t = 0$, 0.2, 0.4, 0.6, 0.8, 1.0, 1.2 and 1.4 if the standard MFE solution of Burgers' equation is repeated with the number of nodes reduced to 21 and with $C_0 = 2 \times 10^{-3}$.

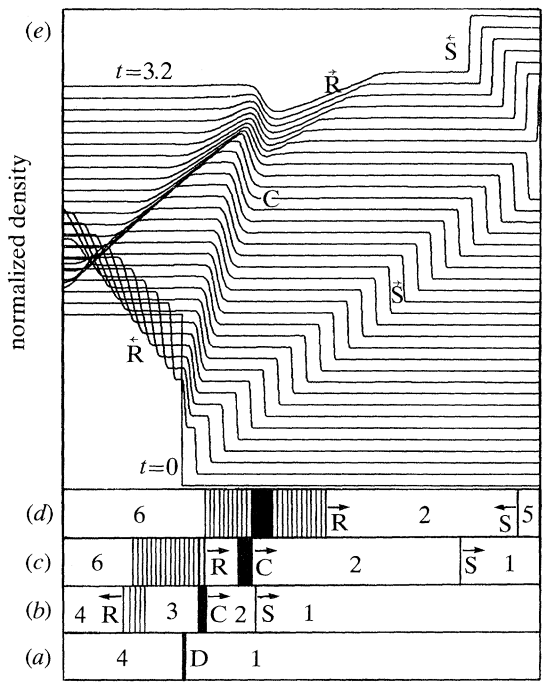

Figure 6. Shock tube at $t = 0$ (a), $t = 0.5$ (b), $t = 2$ (c) and $t = 2.8$ (d) and density profiles within shock tube from $t = 0$ to $t = 3.2$ with $\Delta t = 0.1$ (e). D = diaphragm, R = rarefaction wave, C = contact surface, S = shock wave.

a shock wave travels to the right. The cooling of the gas by the leftward moving rarefaction wave and the heating of the gas by the rightward moving shock produces a jump in temperature and hence in density. This 'contact surface', contained in the

PHILOSOPHICAL TRANSACTIONS OF THE ROYAL SOCIETY A MATHEMATICAL, PHYSICAL & ENGINEERING SCIENCES

constant flow region between the rarefaction and shock waves, travels to the right at the gas velocity. The constant flow regions on either side of the shock, contact surface, and rarefaction wave are labelled 1, 2, 3 and 4, going from right to left. At later times, the shock wave and rarefaction wave reflect off the end walls of the shock tube, creating new constant flow regions 5 and 6 respectively. Owing to the relatively small pressure jump between regions 1 and 4, the temperature change resulting from the passage of the rarefaction and shock waves will not appreciably effect the value of the specific heat ratio: therefore, γ is set to the constant value of 1.4 in the calculations that follow.

(*a*) *Equations*

The set of partial differential equations describing the time evolution of a gas in the one-dimensional domain can be written using density, gas velocity and temperature as the principal variables (denoted ρ, V and T, respectively). To avoid numerical difficulties associated with disparate magnitudes of the solution components, it is desirable to normalize the variables by replacing ρ by ρ/ρ_1, V by V/a_1, T by T/T_1, X by X/L_N and t by $a_1 t/L_N$. ρ_1, a_1 and T_1 are the unnormalized density, speed of sound and temperature in the (undisturbed) low-pressure region and L_N is a normalization length. Note that, because the gas is calorically and thermally perfect, we write $a_1 = \sqrt{(\gamma R T_1)}$, where R is the gas constant. The partial differential equations, assuming that there are no composition changes, no long-range electrical or magnetic interactions, and no body forces, may be written in the form

$$\frac{\partial \rho}{\partial t} = -V\frac{\partial \rho}{\partial X} - \rho\frac{\partial V}{\partial X}, \tag{34}$$

$$\frac{\partial V}{\partial t} = -V\frac{\partial V}{\partial X} - \frac{1}{\gamma\rho}\frac{\partial \rho T}{\partial X} + \frac{2}{Re}\frac{1}{\rho}\frac{\partial^2 V}{\partial X^2} \tag{35}$$

and

$$\frac{\partial T}{\partial t} = -V\frac{\partial T}{\partial X} - [\gamma - 1]\,T\frac{\partial V}{\partial X} + \frac{\gamma}{Re\,Pr}\frac{1}{\rho}\frac{\partial^2 T}{\partial X^2} + \frac{2\gamma[\gamma-1]}{Re}\frac{1}{\rho}\left[\frac{\partial V}{\partial X}\right]^2, \tag{36}$$

where Re is the Reynolds number and Pr is the Prandtl number (constant value of 0.71).

(*b*) *Initial conditions*

The initial profiles for the solution should contain finite gradients with rounded corners. It is convenient to model the density transition as

$$\rho[X] = \bar{\rho} + \tfrac{1}{2}\delta\rho \tanh\left[2[X_D - X]/L_D\right], \tag{37}$$

where X_D is the position of the diaphragm, where L_D is the initial thickness of the pressure transition, and where $\bar{\rho}$ is the average density and $\delta\rho$ is the density change across the diaphragm (equal to 1.5 and 0.5, respectively for this shock-tube problem). A linear-ramp profile can also be used but results in smaller time-steps at early times.

It is desirable to adapt the initial node distribution to the initial conditions for the problem. The nodes are placed, subject to limits on smallest- and largest-allowed node separation, so as to roughly equidistribute the magnitude of the product of the second derivative of the pressure times the square of the node separation. The algorithm used is

$$X^{i\pm1} = X^i \pm \Delta X_{\text{small}}\frac{\sqrt{\epsilon^i_{\max}}}{\sqrt{(\epsilon^i + \sigma\epsilon^i_{\max})}}, \tag{38}$$

where ΔX_{small} is the smallest-allowed node separation, σ is the square of the ratio of the smallest and largest allowed node separations, and

$$\epsilon^i = |\partial^2 P^i / \partial X^2| \tag{39}$$

is an error measure evaluated at node i. $\epsilon^i_{\max}$ is the maximum value of ϵ^i, which occurs at

$$2[X_{\text{D}} - X]/L_{\text{D}} = \pm \ln [\sqrt{(3+1)}/\sqrt{(3-1)}] \approx \pm 0.658, \tag{40}$$

if the 'tanh' density profile is used.

The algorithm is started with a node placed at one of the maxima of the error measure and proceeds in two directions: towards the centre of the pressure transition and towards the adjacent boundary. The node positions at the extremes are adjusted to be equal to the value of X at the boundary and at the centre of the transition. Nodes are placed about the other maxima in the same way. ΔX_{small} is chosen to be several times smaller than L_{D}, which in turn is chosen to be somewhat smaller than the expected equilibrium thickness of the shock. In some cases it is convenient to add or remove nodes 'by hand' to fine tune the initial node distribution.

(c) *Boundary conditions*

Many of the problems solved used the 'reflection' boundary condition at the closed ends of the shock tube. That is, the slope of density and temperature (or density and total energy) was set to zero, while the velocity (or momentum density) was assumed to be antisymmetric and, therefore, equal to zero at the boundary. The effect of this Neumann boundary condition is equivalent to a wave, incident at a boundary, colliding head-on with an identical wave of opposite orientation, so that no gas will flow across the boundary.

An alternative procedure is to specify Dirichlet boundary conditions that impose a similar symmetry. The Dirichlet reflection boundary conditions were adapted from expressions derived by Groth & Gottlieb (1988). The velocity, density, and temperature at the boundary node are expressed in terms of the same quantities at the nearest interior node using expressions derived from the head-on collision of two identical shock waves or two identical rarefaction waves.

(d) *Results of* MFD *calculations*

The MFD method was applied to the shock-tube problem using (34)–(36) with a Reynolds number of about 2500. The solution weights were $\omega_1 = \omega_2 = \omega_3 = 1$ and $\omega_4 = 0$. $\mathcal{Q}'$ was equal to 128 with the maximum-ratio-of-node-separation parameter B set to $\frac{1}{4}$. The penalty-function coefficients were $C_0 = 0$, $C_2 = 1.2 \times 10^{-7}$, $C_3 = 1.9 \times 10^{-3}$ and $C_G = 1/1024$ with powers $C_4 = 3$ and $C_5 = 2$. Dirichlet reflection boundary conditions were specified at the ends of the shock tube.

The initial tanh density profile and node distribution was computed for the domain $X = 0$ to $X = 4$, with $L_{\text{D}} = 10^{-3}$, $X_{\text{D}} = 1$, $\Delta X_{\text{small}} = 1.25 \times 10^{-5}$ and $\sigma = 5 \times 10^{-5}$. The profile originally contained 182 nodes, but this was reduced to 97 nodes by removing every second node except at the extreme left of the domain. This culling procedure produced an especially smooth grid distribution having extra nodes on the left to help round out the corners of the initial rarefaction wave.

Figure 7*a–c* shows plots of density, temperature and pressure within the shock tube at successive time intervals from $t = 0$ to $t = 3.2$. The calculation used about 23 min of CPU time and required the computation of 64 jacobians and a total of 1509 finite-difference evaluations of the right-hand side of (13). At $t = 3.2$, the value of Δt

PHILOSOPHICAL TRANSACTIONS OF THE ROYAL SOCIETY A MATHEMATICAL, PHYSICAL & ENGINEERING SCIENCES

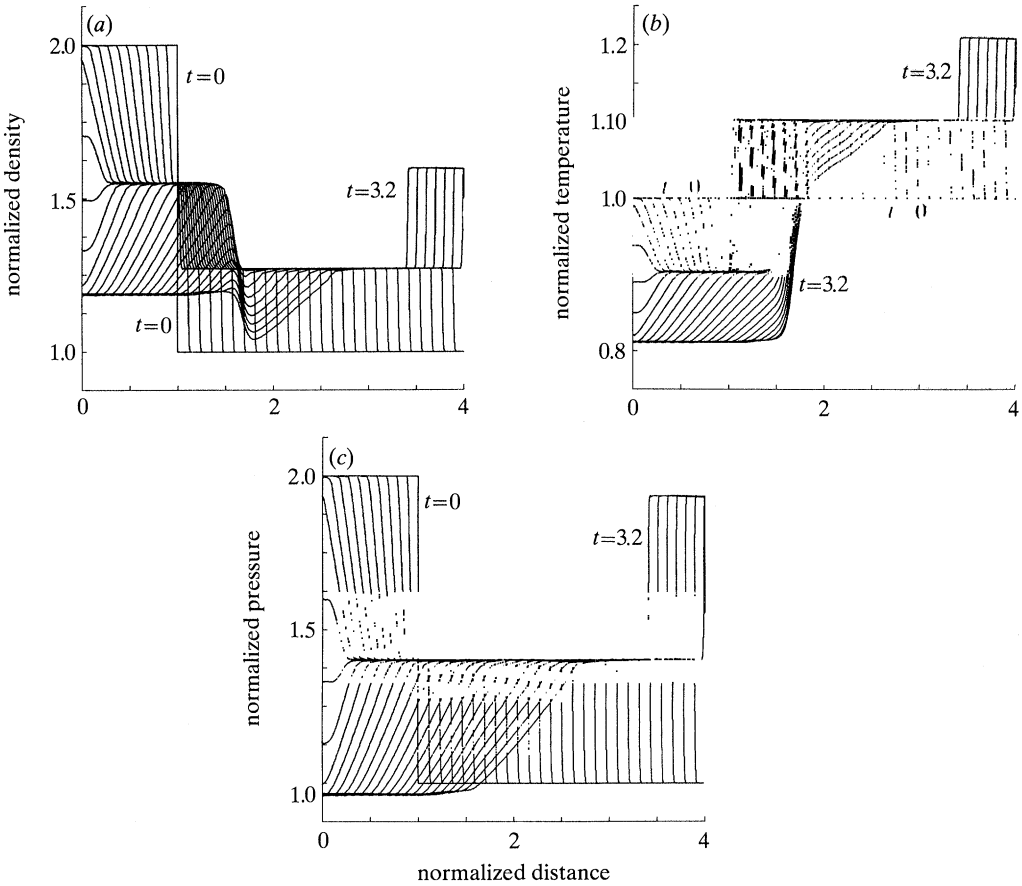

Figure 7. (*a*) Density, (*b*) temperature and (*c*) pressure profiles from $t = 0$ to $t = 3.2$ with $\Delta t = 0.1$, obtained from the standard MFD solution of the shock tube problem. Parameters: 97 nodes, $C_0 = 0$, $C_2 = 1.2 \times 10^{-7}$, $C_3 = 1.9 \times 10^{-3}$, $C_4 = 3$, $C_5 = 2$, $C_G = 1/1024$, $\Omega' = 128$, $B = 0.25$, $\omega_1 = \omega_2 = \omega_3 = 1$, $\omega_4 = 0$, Dirichlet reflection boundary conditions.

was about 0.028 and the fractions of the total integration-time span, which used the first-, second- or third-order EPISODE ODE solution methods were about 0.0009%, 68% and 32% respectively. Note that the value of V_2/a_1 and the ratios of ρ, T and P across the initial and reflected shock waves and rarefaction waves were within a fraction of a percent of the values predicted by inviscid analytical formulae. Also, nearly invisible jumps in the solution occur at the boundaries since the Dirichlet conditions are not strictly correct for a viscid calculation, but the solution elsewhere is not disturbed thereby.

A slight reduction in quality of shock reflection was obtained if the Neumann reflection boundary conditions were imposed instead of Dirichlet reflection boundary conditions; as illustrated in the density profiles of figure 8, fine-scale oscillations of small amplitude are produced.

Calculations of reduced quality using smaller or zero values of Ω' have also been performed. For both versions of the reflection boundary condition, oscillations of increasing size occur in the reflected shock wave as Ω' approaches zero. However, the quality of the calculation before the time of reflection of the shock is excellent. Figure 9 illustrates the density profiles from $t = 0$ to $t = 2.5$ for $\Omega' = 0$ with the penalty

Figure 8

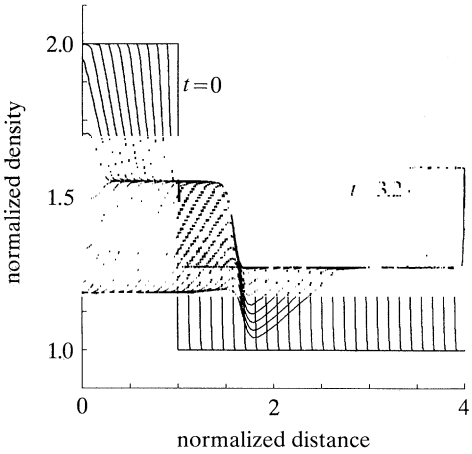

Figure 9

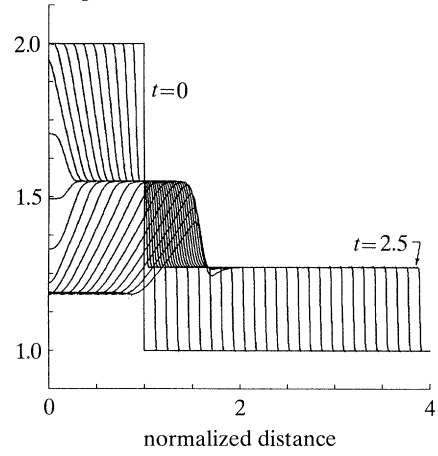

Figure 8. Density profiles from $t = 0$ to $t = 3.2$ with $\Delta t = 0.1$, obtained by repeating the standard MFD solution of the shock tube problem with Neumann reflection boundary conditions.

Figure 9. Density profiles from $t = 0$ to $t = 2.5$ with $\Delta t = 0.1$, obtained by repeating the standard MFD solution of the shock tube problem with altered parameters. Altered parameters: $\Omega' = 0$, $C_2 = 4 \times 10^{-9}$, $C_3 = 9 \times 10^{-5}$.

Figure 10

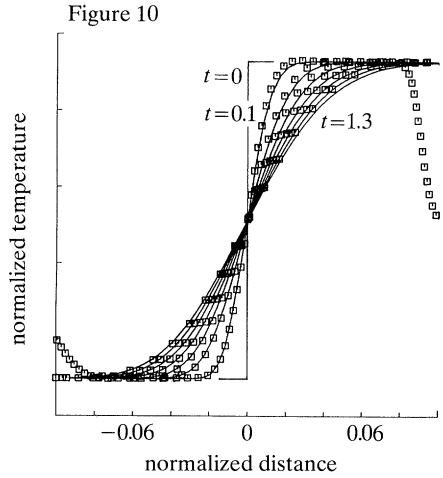

Figure 11

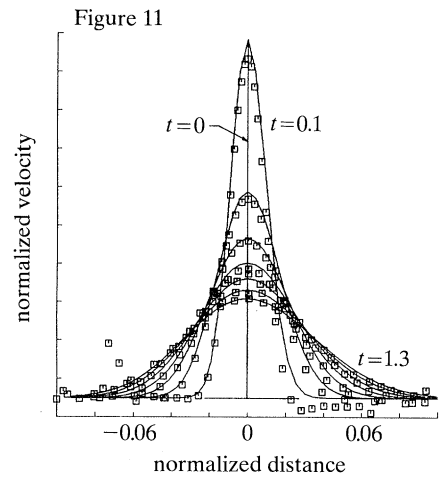

Figure 10. Temperature profiles within the contact surface from MFD calculation. The square symbols represent the numerical solutions at $t = 0.1$, 0.3, 0.5, 0.7, 0.9, 1.1 and 1.3. The solid lines are computed from the analytical formulae of Hall (1954).

Figure 11. Velocity profiles within the contact surface from MFD calculation. The square symbols represent the numerical solutions at $t = 0.1$, 0.3, 0.5, 0.7, 0.9, 1.1 and 1.3. The solid lines are computed from the analytical formulae of Hall (1954) as modified by Hawken (1990).

function coefficients reduced to $C_2 = 4 \times 10^{-9}$ and $C_3 = 9 \times 10^{-5}$. The profiles of the solution within the contact surface and shock wave are compared with analytically derived profiles below.

The solid lines in figure 10 are the profiles of temperature in the contact surface computed for various values of normalized time using the approximate theory of Hall (1954). The square symbols are obtained from the numerical results by transforming to a frame where the contact surface is stationary and centred on the

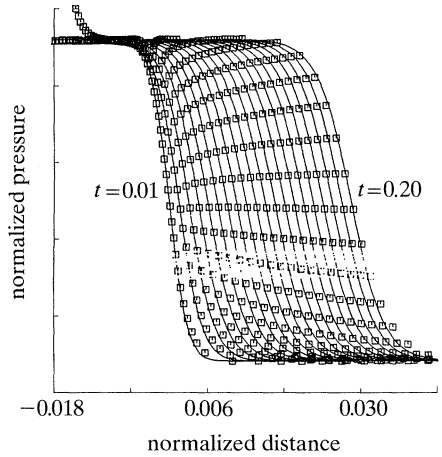

Figure 12. Pressure profiles within the shock wave from MFD calculation. The square symbols represent the numerical solutions from $t = 0.01$ to $t = 0.20$ at intervals of 0.01. The solid lines are computed from the analytical formula of Lighthill (1956) as modified by Honma & Glass (1983).

origin. Good qualitative agreement can be seen. A similar comparison of analytical and numerical values of the velocity profile through a contact surface where the numerical estimate of V_2/a_1 has been subtracted from the numerical results is shown in figure 11. The spread and decay of the velocity hump for the numerical calculation is in good qualitative agreement with the theory of Hall as modified by Hawken (1990). Note that the height of the largest hump in the figure is less than 2 % of V_2/a_1. The greatest systematic disagreements occur on either side of the tallest profile, and this is due to the close proximity of the rarefaction wave, contact surface and shock at $t = 0.1$. The agreement is quite good considering the approximations made by Hall and the fact that the initial conditions of Hall do not exactly match those of the numerical solution.

In figure 12, the solid lines are the pressure profiles through the shock computed using the theory of Lighthill (1956) as modifed by Honma & Glass (1983). The symbols were obtained from the numerical results by transforming to a frame where the origin moves with the centre of the shock. The profiles are displaced slightly relative to one another to maintain clarity of display. In view of the weak shock assumption of Honma & Glass, the agreement is quite good. The, initially, very thin shock profile grows in thickness at very early times to approach the asymptotic profile predicted by Taylor (1910). The tendency for the shock to grow in thickness owing to the influence of heat conduction and viscosity is balanced by the tendency to steepen owing to coalescence of characteristics as the limiting Taylor profile is reached.

Typical minimum node spacings in the vicinity of the shock were about $0.002L_N$. This suggests that a non-adaptive finite-difference method would require at least 2×10^3 nodes to solve the same problem. The MFD method required less than $\frac{1}{20}$ of this number of nodes. Note that node separations as small as $10^{-5}L_N$ have occurred during the reflection of the shock off the end of the shock tube.

Similar calculations with double the Reynolds number have been performed. The quality of the rarefaction waves, contact surface and running shock wave was quite good but the reflected shock wave contained excessive oscillations. For gasdynamic problems in general, the MFD method solution deteriorates if the Reynolds number

PHILOSOPHICAL TRANSACTIONS OF THE ROYAL SOCIETY A MATHEMATICAL, PHYSICAL & ENGINEERING SCIENCES

is much greater than 10^3. This is a limitation shared by the MFE method and is caused by noise generated during numerical estimation of the jacobian of the discretized PDEs. It has been indicated by Djomehri (1983) that if an analytical (laboriously derived) jacobian is used, the Reynolds number can be ten times larger. Even so, the contact-surface thickness will be smaller only by the factor $\sqrt{10}$. Computation of an analytical jacobian is appropriate for a more specialized code than the one developed in the work reported herein.

Calculations, using momentum density, density and total energy per unit volume as the principal variables so that the system of equations could be put in conservation-law form, were only slightly inferior in quality to ones described above but typically required more than a 50% increase in CPU time. Differencing of the leading terms in (34)–(36) enhances the diagonal dominance of the jacobian of (13) and results in larger time-step sizes than if the PDEs were in conservation-law form. Even replacing the right-hand side of (34) by $-\partial(\rho V)/\partial X$, to put it in conservation-law form, increases CPU time.

(e) *Results of MFE calculations*

The MFE method was applied to the shock tube problem using (34)–(36), and the same initial conditions, number of nodes, and initial distribution were used as for the previous MFD calculations. Neumann reflection boundary conditions were specified at each end of the domain. The horizontal-emphasis parameter was 0.65 and the overemphasis-of-viscosity value was set to 1.1. The solution weights were $\omega_1 = \omega_2 = \omega_3 = 1$. The penalty-function coefficients were $C_0 = 0$, $C_2 = 1.4 \times 10^{-8}$, $C_3 = 1.6 \times 10^{-4}$ and $C_G = 1/1024$ with powers $C_4 = 2$ and $C_5 = 1$.

Figure 13*a–c* shows plots of density, temperature, and pressure within the shock tube at successive time intervals. These results are almost as good in quality as those of the previous MFD calculations. However, fewer nodes followed the penetration of the contact surface by the reflected rarefaction than in the MFD calculations; hence, solution quality suffers there.

The temperature profile within the contact surface and pressure profile within the shock wave have alsc been computed and are quite similar to those obtained by the MFD method. However, as is illustrated in figure 14, the velocity profile within the contact surface exhibits a sudden jump in height from one time level to the next. This jump may be indicative of a small-scale instability in the MFE solution.

It took about 48 min of CPU time to reach $t = 3.2$ and required the computation of 164 jacobians and a total of 3544 finite-element evaluations of the right-hand side of (13). At $t = 3.2$, the value of Δt was about 0.012 and the fractions of the total integration-time span which used the first-, second- or third-order EPISODE ODE-solution methods were about 3%, 73% and 23% respectively. The MFE calculations spent a somewhat smaller proportion of time using the higher order EPISODE ODE-solution methods than did the MFD calculations and was somewhat slower.

Since the solution essentially consists of travelling waves of constant amplitude, a large horizontal-emphasis was used to dramatically speed up the calculation without causing deterioration of the solution. A similar calculation with reduced horizontal-emphasis (parameter equal to 0.90), required more than 70 min to reach $t = 3.2$. Transmission of nodes through the contact surface exhibited little change. A similar calculation having a horizontal-emphasis parameter of 1 required more than 80 min to reach $t = 1.1$. Use of larger overemphasis of viscosity also did not significantly improve the solution.

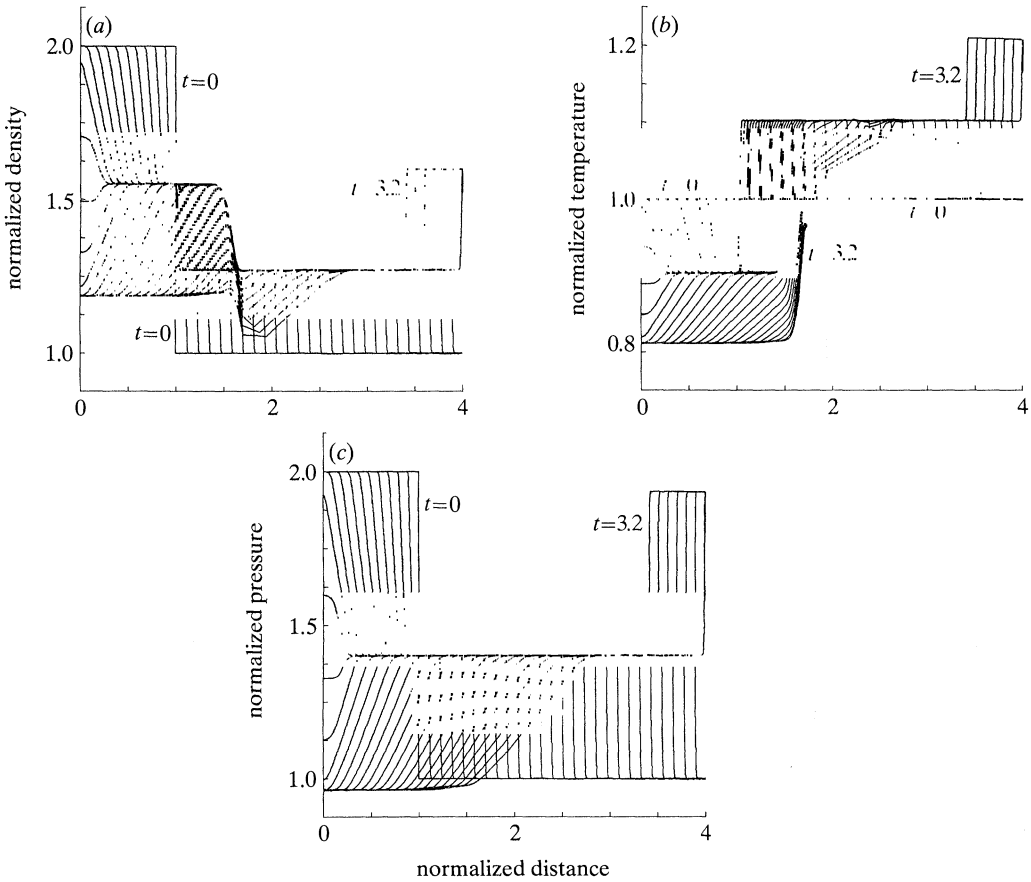

Figure 13. (*a*) Density, (*b*) temperature and (*c*) pressure profiles from $t = 0$ to $t = 3.2$ with $\Delta t = 0.1$, obtained from the MFE solution of the shock tube problem. Parameters: 97 nodes, $C_0 = 0$, $C_2 = 1.4 \times 10^{-8}$, $C_3 = 1.6 \times 10^{-4}$, $C_4 = 2$, $C_5 = 1$, $C_G = 1/1024$, horizontal emphasis = 0.65, and overemphasis of viscosity = 1.1, $\omega_1 = \omega_2 = \omega_3 = 1$, Neumann reflection boundary conditions.

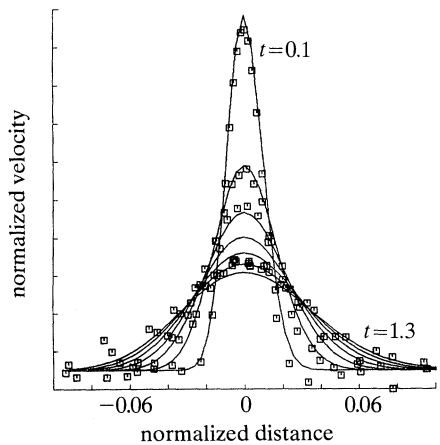

Figure 14. Velocity profiles within the contact surface from MFE calculation. The square symbols represent the numerical solutions at $t = 0.1$, 0.3, 0.5, 0.7, 0.9, 1.1 and 1.3. The solid lines are computed from the analytical formulae of Hall (1954) as modified by Hawken (1990).

10. Rarefaction wave in a duct with an area reduction

In this problem, a rarefaction wave of pressure ratio 0.45, moving in a gas with specific heat ratio 1.4, is incident from the left on an area reduction with A_R/A_L equal to 0.40, as illustrated in figure 15. It causes a flow from right to left through an area increase. This was originally a test case for Gottlieb & Saito (1983) and Gottlieb & Igra (1983). They used the random choice method to solve an inviscid set of equations using density, momentum density and total energy per unit volume as the principal variables.

(a) *Equations*

In the work reported here it has proven beneficial to use velocity, density and temperature as the principal variables. The resulting equations in normalized form are

$$\frac{\partial \rho}{\partial t} = -V\frac{\partial \rho}{\partial X} - \rho\frac{\partial V}{\partial X} - \rho V\frac{\partial \ln A}{\partial X}, \tag{41}$$

$$\frac{\partial V}{\partial t} = -V\frac{\partial V}{\partial X} - \frac{1}{\gamma\rho}\frac{\partial \rho T}{\partial X} + \frac{2}{Re}\frac{1}{\rho}\frac{\partial^2 V}{\partial X^2} \tag{42}$$

and

$$\frac{\partial T}{\partial t} = -V\frac{\partial T}{\partial X} - [\gamma-1]T\frac{\partial V}{\partial X} - [\gamma-1]TV\frac{\partial \ln A}{\partial X} + \frac{\gamma}{RePr}\frac{1}{\rho}\frac{\partial^2 T}{\partial X^2} + \frac{2\gamma[\gamma-1]}{Re}\frac{1}{\rho}\left[\frac{\partial V}{\partial X}\right]^2, \tag{43}$$

where A is the cross-sectional area of the duct. Equations (41) and (43) may be obtained by adding a source term proportional to $\partial \ln A/\partial X$ to (34) and (36). Much smaller source terms, derived from a detailed analysis of diffusion effects, have been neglected since only macroscopic phenomena are of interest for this calculation.

The cross-sectional area to the left of the area change is A_L, whereas that to the right is A_R. The area change has a length of one in normalized spatial coordinates. It is convenient to start the area change at the origin. The cross-sectional area at any point is given by

$$A(X) = \begin{cases} A_L & \text{if} \quad X < 0, \\ A_L \exp\left[\tfrac{1}{2}\ln\left[A_R/A_L\right]\left[1-\cos \pi X\right]\right] & \text{if} \quad 0 \leqslant X \leqslant 1, \\ A_R & \text{if} \quad 1 < X, \end{cases} \tag{44}$$

so that the area at each edge of the transition will blend smoothly with the areas on the left and right sides.

An artificial-viscosity term of the form

$$+\frac{2\mu}{Re}\frac{\partial^2 \rho T}{\partial X^2} \tag{45}$$

was inserted into (41) to suppress fine-scale oscillations in the vicinity of stationary shocks. The artificial viscosity coefficient, μ, was set to 0.4. Reducing the value of μ by a factor of ten causes a slight increase in the amplitude of the oscillations, increases CPU time by about 3%, and does not produce noticeably thinner shocks.

The incident rarefaction wave was modelled as a linear transition in flow velocity with a normalized length of $\frac{5}{6}$ and with the head located at $-\frac{1}{3}$. A total of 97 nodes was used. The nodes were highly concentrated within the rarefaction wave and area

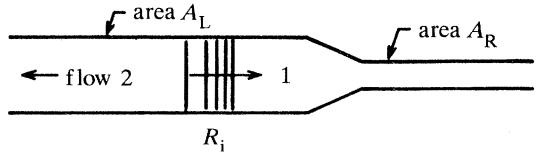

Figure 15. Illustration of a rarefaction wave moving towards an area reduction in a duct.

change but were spread further apart elsewhere. Neumann reflection boundary conditions were used, but the left-hand and right-hand boundaries were placed at $X = -16$ and $X = 14$, respectively, to avoid impingement by waves during the course of the calculation.

The normalized flow velocity to the left of the incident rarefaction wave was computed from P_{21}, the pressure ratio across the rarefaction wave, using the analytical relationship

$$V_{21} = -2[1-[P_{21}]^{[\gamma-1]/2\gamma}]/[\gamma-1]. \tag{46}$$

The initial value of V is made to vary linearly from V_{21} at the tail to 0 at the head of the rarefaction wave, and the initial values for density, and temperature are computed as required from V, using isentropic relations.

(*b*) *Results of* MFD *calculations*

The MFD method was applied to (41) (including the artificial viscosity term), (42) and (43) with the same Reynolds and Prandtl numbers used in the shock tube problem. The solution weights were $\omega_1 = 1$, $\omega_2 = 4$ and $\omega_3 = 1$, with $\omega_4 = 0$. The penalty-function coefficients were $C_0 = 0$, $C_2 = 3 \times 10^{-9}$, $C_3 = 4.8 \times 10^{-4}$ and $C_G = 0.01$ with powers $C_4 = 3$ and $C_5 = 2$. Ω' was equal to 2 with the maximum-ratio-of-node-separation parameter B set to $\frac{1}{4}$. The calculation required 36 min CPU time to reach $t = 13.44$.

Figure 16*a–d* illustrates the MFD spatial profiles of pressure, flow velocity, density and entropy at increasing times. The entropy, S, normalized by the gas constant, R, may be expressed in the form

$$S = -\frac{1}{\gamma-1}\ln\left[\frac{P}{\rho^\gamma}\right]. \tag{47}$$

The entropy of the initially undisturbed right-hand side of the domain is arbitrarily assigned the value of zero, and the density and pressure are normalized by their undisturbed values. The logarithmic entropy function reduces the relative strength of the shock waves so that weak contact surfaces will be readily visible; it also overemphasizes the presence of noise in the numerical solution.

The first portion of the incident rarefaction wave passes through the area reduction to become the transmitted rarefaction wave. A weak reflected rarefaction wave is also visible. Note that the process of transmission and reflection is distributed over the entire area change. The progress of a wave through an area change can be visualized as creating a series of infinitesimally weak reflected and re-reflected disturbances that eventually coalesce. The transmitted and reflected waves eventually leave the area change and a steady flow is established asymptotically with time.

A flow is set up that is just sonic at the right-hand side of area change. This flow is accelerated to supersonic speed by a portion of the incident rarefaction wave still

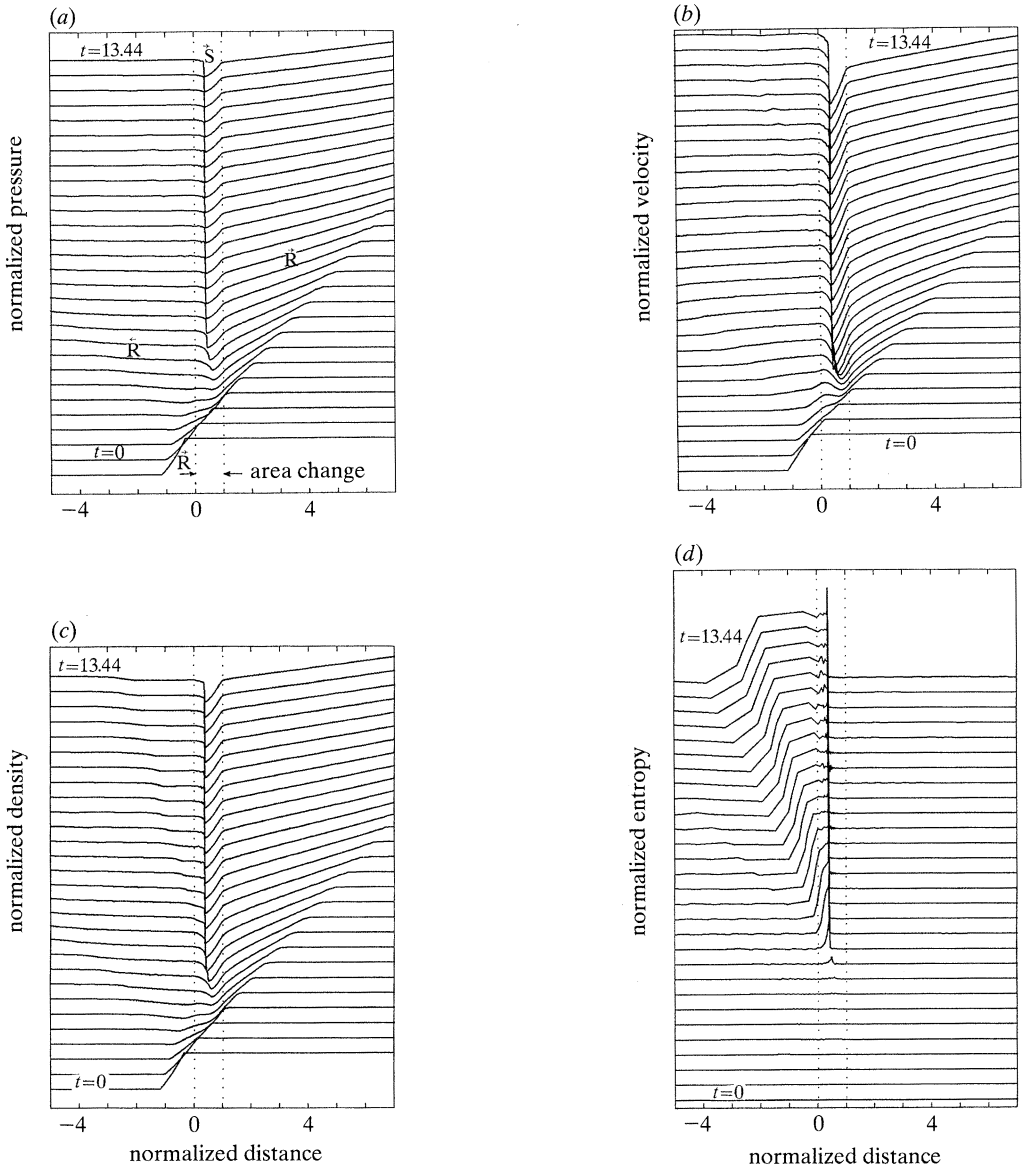

Figure 16. MFD spatial profiles of (*a*) pressure, (*b*) flow velocity, (*c*) density and (*d*) entropy for the interaction of a rarefaction wave with an area reduction from $t = 0$ to $t = 13.44$ with $\Delta t = 0.48$. Only part of the computational domain is shown. ($P_2/P_1 = 0.45$, $A_R/A_L = 0.40$) MFD parameters: 97 nodes, $C_0 = 0.0$, $C_2 = 3 \times 10^{-9}$, $C_3 = 4.8 \times 10^{-4}$, $C_4 = 3$, $C_5 = 2$, $C_G = 0.01$, $\Omega' = 2$, $B = 0.25$, $\omega_1 = 1$, $\omega_2 = 4$, $\omega_3 = 1$, $\omega_4 = 0$.

within the area change and the effects of increasing area on the flow. An upstream-facing recompression shock wave forms within the area change and decelerates the oncoming flow to a subsonic speed, which is further reduced by the remaining area increase. The formation of this recompression shock causes a spatially distributed contact surface of changing entropy and density which is swept downstream (most readily seen in the entropy plot).

On the whole the solution is of high quality and is in good agreement with the

Figure 17

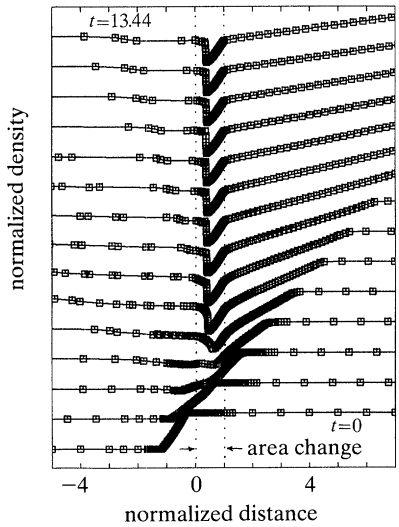

Figure 18

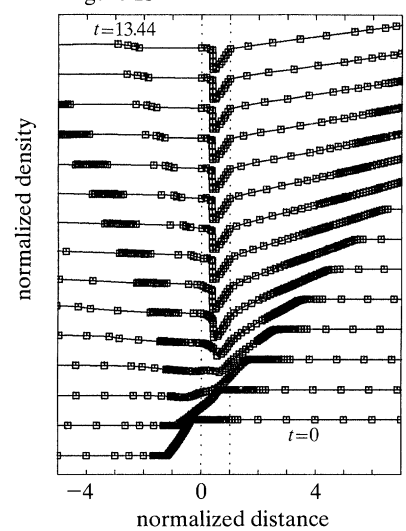

Figure 17. MFD spatial profiles of density and node distributions at $t = 0$, 0.96, 1.92, 2.88, 3.84, 4.80, 5.76, 6.72, 7.68, 8.64, 9.60, 10.56, 11.52, 12.48 and 13.44 resulting from the calculation described in figure 16.

Figure 18. MFD distributions that typically occur for the interaction of a rarefaction wave with an area reduction if $\Omega' = 0$. $t = 0$, 0.96, 1.92, 2.88, 3.84, 4.80, 5.76, 6.72, 7.68, 8.64, 9.60, 10.56, 11.52, 12.48 and 13.44.

results of Gottlieb & Igra (1983). However, the solution of this particular problem does illustrate a weakness of adaptive methods. Few nodes remain in the vicinity of the contact surface because the change in density or temperature across the contact surface is much smaller than the change across the other waves. The change in entropy at the contact surface is the same as in the results of Gottlieb & Igra but the nodes in the vicinity of the contact surface slowly drift apart in response to forces external to the (very weak) contact surface. The resultant accelerated thickening of the contact surface is most clearly illustrated by the spatial profiles of entropy. Relative lack of resolution of very weak waves would seem likely to be common to all adaptive methods. Whether lack of resolution of very weak waves is a serious problem is dependent on what use the results of an adaptive calculation will be applied. A short-lived disturbance in the MFD velocity profiles may be a result of the reduced node concentration at the contact surface. Figure 17 shows typical node distributions within the density profiles at various times.

If ω_3 is increased to 4 or if ω_2 is reduced to 1, the solution profiles are slightly noisier. Doubling the Reynolds number also increases the noise in the solution profiles but does not otherwise result in a noticeable change in the thickness of waves.

If Ω' is set to zero, then, as illustrated in figure 18, there is a great reduction of node concentration in the interior of the stationary shock. (However, the CPU time is reduced to about 19 min.) The nodes are swept towards the periphery of the computational domain. The inadequately resolved recompression shock develops disturbances. Increasing C_3 relative to C_2 can decrease the loss of nodes from the shock, but this also prevents sufficient spread of nodes to resolve the behaviour of the transmitted rarefaction wave. The Ω' terms are crucial to obtaining good solutions to problems involving interactions of waves with area changes. The Ω' terms

counteract the tendency of the nodes to follow the characteristics of the solution which in this case would cause most nodes to follow the moving flow features.

(c) *Results of* MFE *calculations*

The MFE method was applied using the same initial conditions as those used in the MFD calculations. The solution weights were $\omega_1 = 1$, $\omega_2 = 4$ and $\omega_3 = 1$. The penalty-functions coefficients were $C_0 = 0.0005$, $C_2 = 6 \times 10^{-9}$, $C_3 = 0.64$ and $C_G = 0.01$ with powers $C_4 = 2$ and $C_5 = 1$. The calculation required about 25 min CPU time to reach $t = 13.44$.

As illustrated in figure 19, the large value of C_3/C_2 was unable to force retention of a sufficient number of nodes within the stationary shock, and yet this still prevented nodes from spreading to properly resolve the transmitted rarefaction. Hence, there are oscillations propagating away from the recompression shock. The horizontal-emphasis parameter was given a value of 0.65. This had the effect of slightly increasing node spread to the right of the area change and of increasing the execution speed to about eight times the value it would otherwise have been. Terms analogous to the Ω terms of the MFD method have not yet been developed, but they might improve the performance of the MFE method for such area-change problems.

11. Shock wave in a duct with an area enlargement

As illustrated in figure 20, a shock wave of Mach 1.80 in a gas with specific heat ratio 1.4 impinges from the left on an area enlargement with A_L/A_R equal to 0.667. This was originally a test of Greatrix & Gottlieb (1982), who used the random choice method to solve an inviscid set of equations using density, momentum density, and total energy per unit volume as the principal variables.

(a) *Initial conditions*

An attempt was made to use discontinuous initial conditions similar to those used by Greatrix & Gottlieb. That is, the shock was initially located between two adjacent nodes. The initial values of the solution at the nodes ahead of the shock are set to correspond to air at standard temperature and pressure with zero flow velocity. For a shock with an initial Mach number U_S moving into a stationary gas, the normalized pressure at the nodes behind the shock can be calculated in terms of P_{21}, the pressure ratio through the shock, using the analytical Hugoniot relation (Zel'dovich & Raizer 1966), that is

$$P_{21} = \frac{2\gamma[U_S]^2}{\gamma+1} - \frac{\gamma-1}{\gamma+1}. \tag{48}$$

The initial values in normalized form behind the shock wave of velocity, density and temperature can be computed from P_{21} as required using

$$\frac{V_2}{a_1} = \frac{2[P_{21}-1]}{\sqrt{[2\gamma[\gamma-1+[\gamma+1]P_{21}]]}}, \tag{49}$$

$$\rho_{21} = \frac{\gamma-1+[\gamma+1]P_{21}}{\gamma+1+[\gamma-1]P_{21}} \tag{50}$$

and

$$T_{21} = \frac{\gamma+1+[\gamma-1]P_{21}}{\gamma+1+[\gamma-1]/P_{21}}. \tag{51}$$

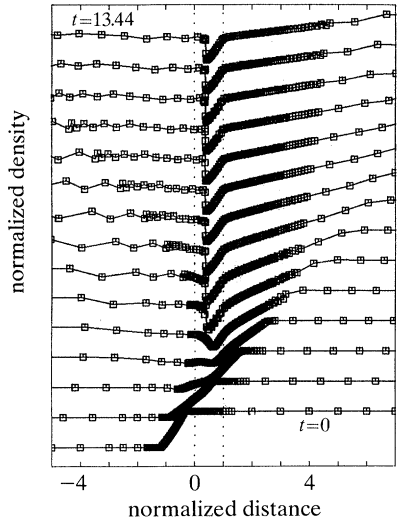

Figure 19. MFE spatial profiles of density and node distributions at $t = 0, 0.96, 1.92, 2.88, 3.84, 4.80, 5.76, 6.72, 7.68, 8.64, 9.60, 10.56, 11.52, 12.48$ and 13.44 resulting from the interaction of a rarefaction wave with an area reduction. ($P_2/P_1 = 0.45$, $A_R/A_L = 0.40$) MFE parameters: 97 nodes, $C_0 = 0.0005$, $C_2 = 6 \times 10^{-9}$, $C_3 = 0.64$, $C_4 = 2$, $C_5 = 1$, $C_G = 0.01$, horizontal emphasis = 0.65, overemphasis of viscosity = 1, $\omega_1 = 1$, $\omega_2 = 4$, $\omega_3 = 1$.

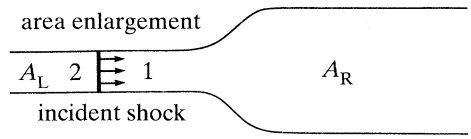

Figure 20. Illustration of a normal shock wave moving in a channel before its impingement on a smooth area change.

The MFD method was used to solve (41)–(43) with the same Reynolds number and Prandtl number as were used in the shock-tube problem and with the nodes distributed so that they were separated by a distance of 10^{-5} in the vicinity of the shock. Nodes tended to enter the shock as the solution developed, so as to model the transition. The nodes were sufficiently close together that Gibbs' oscillations did not develop. Unfortunately the size of the time-step was quite small because of the tendency of nodes to migrate into the shock.

Much larger time-steps are obtained if the initial transition already contains many nodes. As a result of much experimentation, it was determined that the most satisfactory results could be obtained by imposing a Taylor profile on the initial transition. After a value of Reynolds number is chosen, the initial pressure profile is modelled using the hyperbolic tangent expression of Taylor given by (37) (if ρ is replaced by P), with the initial thickness L_D set to the Taylor thickness and with the centre of the shock placed at $X = -\frac{7}{6}$. The nodes are distributed using the procedure described in §9*b*. The values of velocity, density and temperature at a node are computed using equations (49)–(51), with P_{21} replaced by the value of P at the node.

The MFD method is used to solve (41)–(43) using the Taylor-profile initial conditions. As the calculation progresses the initial shock wave separates into a shock wave and a trailing weak pressure pulse with an intervening contact surface. The separation occurs for two reasons. The first is that (49)–(51) are exact only when applied from the front of the shock to its rear. Secondly, a number of approximations

are required to derive the Taylor profile. Thus, the Taylor profile does not match the (more exact) numerical profile, as is clearly shown in the shock-profile figures of §9. The contact surface and pressure pulse are generated as the result of a minor re-adjustment of the solution within the shock wave. The ratios across the readjusted shock wave remain within 0.1% of their initial values.

The calculation is allowed to proceed until $t = 0.22$, at which time the shock has clearly separated from the trailing contact surface but has not yet reached the area change. The nodes on either side of the shock wave, and every second node within the shock wave, are removed. Replacement nodes having the shock-head and shock-tail values of the solution are distributed on either side of the shock to form the initial conditions (without pressure pulse or contact surface) for subsequent calculations. Neumann reflection boundary conditions are used, but the left-hand and right-hand boundaries are placed at $X = -5$ and $X = 34$, respectively, to avoid impingement by waves during the course of the calculation.

(*b*) *Results of* MFD *calculations*

The MFD method was applied to (41) (including the artificial viscosity term), (42) and (43), with initial conditions at $t = 0.22$ generated for a Reynolds number of about 250 and Prandtl number of 0.71. The Reynolds number was ten times smaller than that used in the shock-tube problem; however, note that the domain was about ten times larger, resulting in the same ratio of shock thickness to size of the domain. A total of 94 nodes were used. The solution weights were $\omega_1 = 1$, $\omega_2 = 4$, and $\omega_3 = 4$, with $\omega_4 = 0$. Ω' was equal to 4096 with the maximum-ratio-of-node-separation parameter B set to $\frac{1}{4}$. The penalty-function coefficients were $C_0 = 0$, $C_2 = 6.4 \times 10^{-5}$, $C_3 = 8$ and $C_G = 0.004$ with powers $C_4 = 3$ and $C_5 = 2$. The large values of C_2 and C_3 were required to balance the very large value of Ω'. The calculation required 77 min execution time to reach $t = 18.48$. At $t = 18.48$, the value of Δt was about 0.073 and the fractions of the total integration-time span, which used the first-, second-, third- and fourth-order EPISODE solution methods, were about 4%, 64%, 32% and 0.003% respectively.

The artificial viscosity coefficient, μ, was set equal to 0.03, just about as large a value as could be used without disturbing the solution. If μ was doubled, then the execution speed was considerably faster, but the incident shock would emit a contact surface and become slightly stronger as the solution profile within the shock adjusted to the modification of (41). Much larger values of μ caused a marked departure from the solution ratios predicted by (49)–(51). If μ was reduced to 0.01, no difference in the incident shock was discernible, but the amount of noise in the MFD solution was slightly increased and the execution speed was reduced by about 38%.

Figure 21 *a–d* shows the resultant spatial profiles of pressure, flow velocity, density, and entropy at various times. The incident shock is transmitted through the area enlargement, leaving a reflected rarefaction wave with tail attached to the area-change inlet. At early times, the entropy profiles reveal a contact surface trailing the transmitted shock wave. The contact surface is produced by the weakening of the incident shock as it is transmitted through the area enlargement. At later times, the formation of an upstream-facing shock wave which is swept downstream causes a region of increased entropy to be extended downstream of the upstream-facing shock wave. The leading edge of the increased entropy region constitutes a second contact surface.

At late times, the following flow behaviour is seen. The oncoming flow is

PHILOSOPHICAL TRANSACTIONS OF THE ROYAL SOCIETY A MATHEMATICAL, PHYSICAL & ENGINEERING SCIENCES

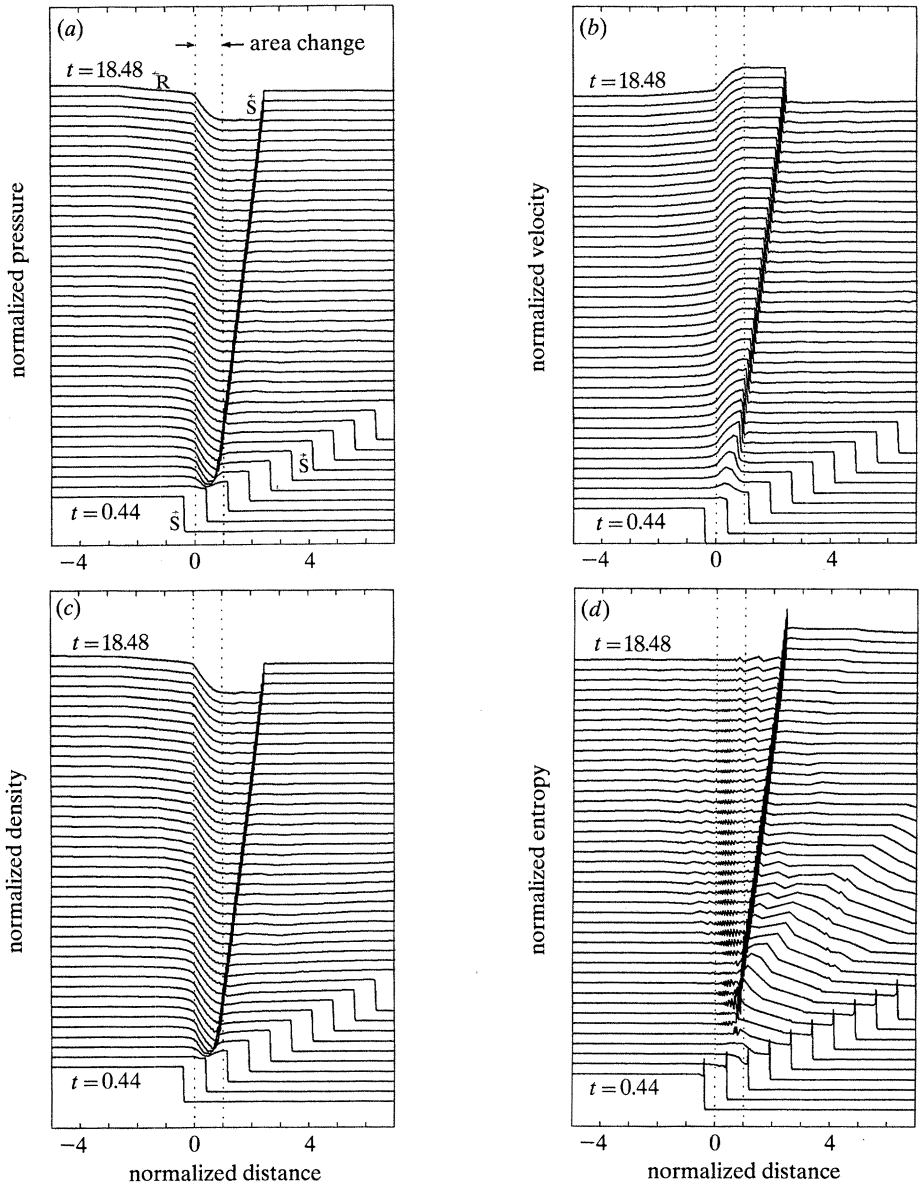

Figure 21. MFD spatial profiles of (*a*) pressure, (*b*) flow velocity, (*c*) density and (*d*) entropy for the passage of a shock wave through an area enlargement for $t = 0.44$ to $t = 18.48$ with $\Delta t = 0.44$. Only part of the computational domain is shown. ($U_S = 1.80$, $A_L/A_R = 0.667$.) Parameters: 94 nodes, $C_0 = 0$, $C_2 = 6.4 \times 10^{-5}$, $C_3 = 8$, $C_4 = 3$, $C_5 = 2$, $C_G = 0.004$, $\Omega' = 4096$, $B = 0.25$, $\omega_1 = 1$, $\omega_2 = \omega_3 = 4$, $\omega_4 = 0$.

accelerated to sonic speed at the area-change inlet by the reflected rarefaction. The area enlargement causes a further acceleration to supersonic speed at the outlet of the area change. A region of quasi-steady supersonic flow exists between the outlet and the upstream-facing shock wave, which is slowly swept downstream. A quasi-steady subsonic flow exists between the upstream-facing shock wave and the originally transmitted shock.

Figure 22

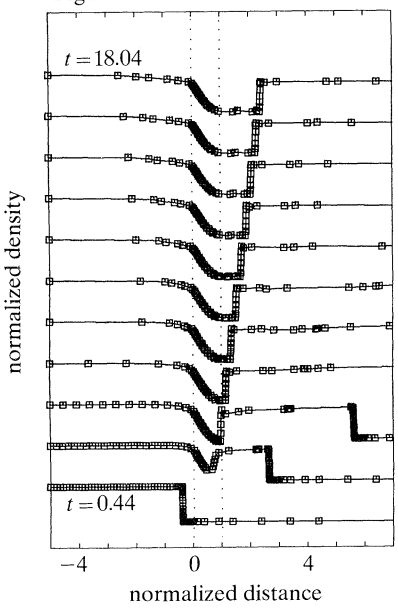

Figure 23

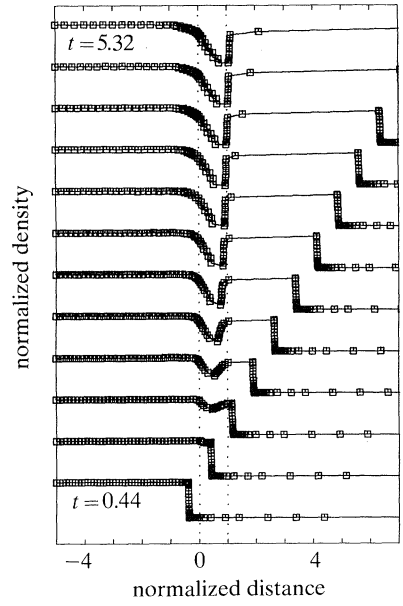

Figure 22. MFD spatial profiles of density and node distributions at $t = 0.44$, 2.20, 3.96, 5.72, 7.48, 9.24, 11.00, 12.76, 14.52, 16.28 and 18.04 resulting from the calculation described in figure 21.

Figure 23. MFD spatial profiles of density and node distributions that typically result from calculations, with Ω' equal to zero, of the passage of a shock wave through an area enlargement. $t = 0.44$, 0.88, 1.32, 1.76, 2.20, 2.64, 3.08, 3.52, 3.96, 4.40, 4.88 and 5.32.

The MFD calculation cannot anticipate the development of the upstream-facing shock and, as shown in figure 22, does not concentrate nodes quickly enough after the development of the shock to prevent a few kinks at the top of the shock at early times. However, the node distribution improves significantly after the upstream-facing shock wave has completely formed.

The spatial profiles of pressure, flow velocity and density are in good agreement with those of Greatrix & Gottlieb (1982). However, since the change in density and temperature across the contact surfaces is so small, the MFD algorithm does not concentrate nodes there. The spreading of nodes and the relatively small Reynolds number combine to produce contact surfaces that are quite thick as compared with those produced by the calculations of Greatrix & Gottlieb. However, these contact surfaces are so weak that they are not readily discernible except in the spatial profiles of entropy.

Despite use of a relatively small Reynolds number, the shock waves are quite thin. The entropy maxima within the shock waves, caused by heat conduction discussed, for example, in Zel'dovich & Raizer (1966), are clearly resolved.

If the MFD calculation is repeated with reduced ω_2 or ω_3, the contact surfaces become less monotone because sensitivity to the weak contact surface is even further reduced. However, an increase in ω_2 or ω_3 does not result in significant improvement at the contact surfaces, but rather causes oscillations near the upstream-facing shock.

Similar MFD calculations have been performed with the Reynolds number increased by a factor of five. The initial contact surface was still not quite as thin as in the calculations of Greatrix & Gottlieb at early times and was quickly spread out

PHILOSOPHICAL TRANSACTIONS OF THE ROYAL SOCIETY A MATHEMATICAL, PHYSICAL & ENGINEERING SCIENCES

by the failure of nodes to concentrate about the very weak density transition. There was also considerable kinking at the top of the upstream-facing shock wave. Execution speed was reduced by a factor of at least 50%.

The very large values of Ω' were required to maintain an acceptable concentration of nodes at the head and tail of the upstream-facing shock. Figure 23 exhibits the inferior node distribution typical of that obtained for calculations in which Ω' is set to zero. In contrast to the results that were reported in §10*b*, runs in which Ω' was of the order of unity were little better.

An MFD calculation of a shock incident on an area enlargement was not performed but the results are expected to resemble those of an MFD calculation with Ω' equal to zero.

12. Concluding remarks

A newly developed MFD method with adaptive movement of nodes has been presented, tested by means of a number of simple but good test problems, and compared in formulation and performance with the MFE method of Miller (1981) and Miller & Miller (1981). The MFD and MFE methods both move the nodes essentially along the solution characteristics, except as modified by penalty functions and (for the MFD method) Ω terms. The new Ω terms developed for the MFD method result in marked improvements in the adaptive node distribution, especially when the flow contains stationary wave phenomena, as often occurs when shock and rarefaction waves interact with area changes. Other benefits of the use of the Ω term include improvement of shock-wave reflection from solid boundaries and increased smoothness at the start and end of transitions through shock waves. Analogous terms could be developed to improve the performance of the MFE method, but this would still leave the MFE method with much longer CPU times for solving most problems (because of the smaller time-steps that the MFE method uses and because of the expense of computing integrals inherent to the MFE method). The solution-component weights ω_1 through ω_K of the MFD method may usually be set to unity with adequate results although small improvements can be achieved by using slightly dissimilar weights, as was done for interactions of shock and rarefaction waves with area changes, and a spherical implosion/explosion problem reported by Hawken (1990).

The adaptive movement of nodes in both the MFD and MFE methods results in the use of fewer nodes and significantly reduced CPU times for computing solutions to problems governed by hyperbolic partial differential equations. However, these advantages are partly offset by the increased difficulty to the user in selecting a good initial distribution of nodes at the start of the computations, and also in selecting appropriate values of coefficients associated with penalty functions and Ω terms. Although good selections of the initial node distribution and values of the penalty functions and Ω-term coefficients can greatly reduce the computational effort, this is difficult because they are normally problem dependent. This frequently leads to an undesirable trial-and-error procedure for their selection. Hence, future research should not only concentrate on developing improved and newer error measures for moving nodes, but it should also be aimed at developing appropriate methods such as automatic procedures for selecting or specifying the resulting coefficients.

The present developments of the MFD method have been directed solely at solving one-dimensional problems with two independent variables (e.g. time and space). This is often useful before undertaking developments of solving multi-dimensional

PHILOSOPHICAL TRANSACTIONS OF THE ROYAL SOCIETY A MATHEMATICAL, PHYSICAL & ENGINEERING SCIENCES

problems, even though some one-dimensional problems do not carry over to multi-dimensional problems. In regards to multi-dimensional problems, it is anticipated that the MFD method will have advantages of computational efficiency similar to those of the MFE method. However, we note here that the original expectations of the MFE method in the early 1980s have not been fulfilled for solving multi-dimensional problems as indicated by Miller (1986); two-dimensional MFE calculations do not exhibit the large gains in computational efficiency typical of one-dimensional MFE calculations except for some simple specialized problems and robust adaptive algorithms for good node movement in two dimensions are not yet available. Hence, the multi-dimensional MFE method has not found widespread application. According to Zegeling & Blom (1990), a major difficulty in two-dimensional MFE calculations is that the tendency of the nodes to follow the solution characteristics can cause entanglement of the grid lines; the Ω terms developed for this paper should offer a method of overcoming the problem for a two-dimensional MFD method.

Financial assistance from the Natural Sciences and Engineering Research Council of Canada was very helpful and is gratefully acknowledged.

References

Anderson, D. A. 1983 Adaptive grid methods for partial differential equations. In *Advances in grid generation* (ed. K. N. Ghia & U. Ghia), pp. 1–15. New York: ASME.

Burgers, J. M. 1948 A mathematical model illustrating the theory of turbulence. *Adv. appl. Mech.* **1**, 171–199.

Byrne, G. D. 1979 The ODE solver EPISODE, its variants, and their use. In *Proc. ANS Topical Meeting on computational methods in nuclear engineering*, pp. 8.17–8.52. Williamsburg, Virginia, U.S.A.

Byrne, G. D. & Hindmarsh, A. C. 1975 A polyalgorithm for the numerical solution of ordinary differential equations. *ACME Trans. math. Software* **1**, 71–96.

Dhomehri, J. 1983 Moving finite element solution of systems of partial differential equations in 1-dimension. *Technical Rep. no. PAM-125*. Center for Pure and Applied Mathematics, University of California.

Djomehri, J. & Miller, K. 1981 A moving finite element code for general systems of PDE's in 2-D. *Technical Rep. No. PAM-57*. Center for Pure and Applied Mathematics, University of California.

Eiseman, P. R. 1987 Adaptive grid generation. *Comput. Meth. appl. Mech. Engng* **64**, 321–376.

Gear, C. W. 1971 *Numerical initial value problems in ordinary differential equations*, ch. 9 and 11. New Jersey: Prentice-Hall.

Gelinas, R. J. & Doss, S. K. 1981 The moving finite element method: a semiautomatic solver for diverse PDE applications. Reprint for 4th IMACS Int. Symp. on computer methods for partial differential equations. Lehigh University, Bethlehem, Pennsylvania.

Gelinas, R. J. & Doss, S. K. 1982 The moving finite-element method: one-dimensional transient flow applications. In *Proc. 10th IMACS World congress on system simulation and scientific computation*, pp. 156–158. Amsterdam: North-Holland.

Gelinas, R. J. & Doss, S. K. 1983 The moving finite element method: strong shock and penetration applications. *Lecture Notes in Engineering*, vol. 3, pp. 192–209. New York and Berlin: Springer-Verlag.

Gelinas, R. J., Doss, S. K. & Carlson, N. N. 1982 Moving finite element research, physical versus non-physical dissipation effects. In *Proc. semi-annual Defence Nuclear Agency airblast review meeting*. Marina del Rey, California, U.S.A: R & D Associates.

Gelinas, R. J., Doss, S. K. & Miller, K. 1981 The moving finite element method: applications to general partial differential equations with multiple large gradients. *J. Comput. Phys.* **40**, 202–249.

PHILOSOPHICAL TRANSACTIONS OF THE ROYAL SOCIETY A MATHEMATICAL, PHYSICAL & ENGINEERING SCIENCES

Gelinas, R. J., Doss, S. K., Vajk, J. P., Djomehri, J. & Miller, K. 1982 Moving finite elements in 2-D. In *Proc. 10th IMACS World congress on system simulation and scientific computation,* pp. 58–60. Amsterdam: North-Holland.

Gottlieb, J. J. & Igra, O. 1983 Interaction of rarefaction waves with area reductions in ducts. *J. Fluid Mech.* **137**, 285–305.

Gottlieb, J. J. & Saito, T. 1983 An analytical and numerical study of the interaction of rarefaction waves with area changes in ducts, Part 1: Area Reductions. *UTIAS Rep. no. 272.* University of Toronto.

Greatrix, D. R. & Gottlieb, J. J. 1982 An analytical and numerical study of a shock wave interaction with an area change. *UTIAS Rep. no. 268.* University of Toronto.

Groth, C. P. T. & Gottlieb, J. J. 1988 Numerical study of two-stage light-gas hypervelocity projectile launchers. *UTIAS Rep. no. 327.* University of Toronto.

Hall, J. G. 1954 The transition through a contact region. *UTIAS Rep. no. 26.* University of Toronto.

Hawken, D. D. 1990 Adaptive node movement in finite-element and finite-difference solutions of partial differential equations with applications to gasdynamics. *UTIAS Rep. no. 333.* University of Toronto.

Hawken, D. F., Gottlieb, J. J. & Hansen, J. S. 1991 Review of some adaptive node-movement techniques in finite-element and finite-difference solutions of partial differential equations. *J. Comput. Phys.* **95**, 254–302.

Hindman, R. G. & Spencer, J. 1983 A new approach to truly adaptive grid generation. *AIAA paper* no. 83-0450, 1–12.

Hindmarsh, A. C. 1979 A collection of software for ordinary differential equations. In *Proc. ANS Topical Meeting on computational methods in nuclear engineering,* pp. 8.1–8.15. Williamsburg, Virginia, U.S.A.

Honma, H. & Glass, I. I. 1983 Random choice solutions for weak spherical shock-wave transitions of N-waves in air with vibrational excitation. *UTIAS Rep. no. 253.* University of Toronto.

Lighthill, M. J. 1956 Viscosity effects in sound waves of finite amplitude. In *Surveys in mechanics* (ed. G. K. Batchelor & R. M. Davies), pp. 250–351. Cambridge University Press.

Miller, K. 1981 Moving finite elements. II. *SIAM J. numer. Analysis* **18**, 1033–1057.

Miller, K. 1983 Alternate modes to control the nodes in the moving finite element method. In *Adaptive computational methods for partial differential equations* (ed. I. Babuska, J. Chandra & J. E. Flaherty), pp. 165–182. Philadelphia: SIAM.

Miller, K. 1986 Recent results on finite element methods with moving nodes. In *Accuracy estimates and adaptive refinements in finite element computations* (ed. I. Babuska, O. C. Zienkiewicz, J. Gago & E. R. de A. Oliveira), pp. 325–338. Chichester: John Wiley and Sons.

Miller, K. & Miller, R. N. 1981 Moving finite elements. I. *SIAM J. numer. Analysis* **18**, 1019–1032.

Rai, M. M. & Anderson, D. A. 1982 Application of adaptive grids to fluid-flow problems with asymptotic solutions. *AIAA J.* **20**, 496–502.

Rai, M. M. & Anderson, D. A. 1980 Grid evolution in time asymptotic problems. In *Numerical grid generation techniques* (ed. R. E. Smith). (*Proc. Numerical Grid Generation Workshop at Langley Research Center*), pp. 409–430. NASA CP-2166.

Taylor, G. I. 1910 The conditions necessary for discontinuous motion in gases. *Proc. R. Soc. Lond.* A **84**, 371–377.

Thompson, J. F. 1984 Grid generation techniques in computational fluid dynamics. *AIAA J.* **22**, 1505–1523.

Thompson, J. F. 1985 A survey of dynamically-adaptive grids in the numerical solution of partial differential equations. *Appl. numer. Math.* **1**, 3–27.

Thompson, J. F., Warsi, Z. U. A. & Mastin, C. W. 1982 Boundary-fitted coordinate systems for numerical solution of partial differential equations. A review. *J. Comput. Phys.* **47**, 1–108.

Thompson, J. F., Warsi, Z. U. A. & Mastin, C. W. 1985 *Numerical grid generation.* New York: North-Holland.

Turkel, E. 1983 Progress in computational physics. *Comput. Fluids* **11**, 121–144.

Zegeling, P. A. & Blom, J. G. 1990 A note on the grid movement induced by MFE. *Rep. no. NM-*

PHILOSOPHICAL TRANSACTIONS OF THE ROYAL SOCIETY A MATHEMATICAL, PHYSICAL & ENGINEERING SCIENCES

R9019. Amsterdam Department of Numerical Mathematics, Centre for Mathematics and Computer Science.

Zel'dovich, Y. B. & Raizer, Y. P. 1966 *Physics of shock waves and high temperature hydrodynamic phenomena*, vols 1 and 2, ch. 1 and 7. New York and London: Academic Press.

Received 14 January 1991; revised 14 June 1991; accepted 3 June 1992

PHILOSOPHICAL TRANSACTIONS OF THE ROYAL SOCIETY A MATHEMATICAL, PHYSICAL & ENGINEERING SCIENCES